

國立交通大學

光電工程研究所

碩士論文

應用於高密度光儲存系統讀取信號之模擬

**Optical Readout Waveforms Simulation in
High Density Optical Storage System**

研究生：高維樑

指導教授：田仲豪 博士

中華民國九十五年七月

應用於高密度光儲存系統讀取信號之模擬

Optical Readout Waveforms Simulation in High Density Optical Storage System

研究生：高維樑
指導教授：田仲豪

Student: Wei-Liang Kao
Advisor: Dr. Chung-Hao Tien

國立交通大學 電機學院

光電工程研究所

碩士論文

A Thesis

Submitted to Institute of Electro-Optical Engineering
College of Electrical Engineering and Computer Science
National Chiao-Tung University
in Partial Fulfillment of the Requirements
for the Degree of
Master
In
Electro-Optical Engineering

June 2006

Hsin-Chu, Taiwan, Republic of China

中華民國九十五年七月

應用於高密度光儲存系統讀取信號之模擬

研究生：高維樑

指導教授：田仲豪博士

國立交通大學 光電工程研究所

摘要

隨著對於儲存容量需求的增加，光儲存系統採用較短的波長以及較高的數值孔徑的物鏡，來達成此一目的。但當較高數值孔徑的物鏡被採用時，光的向量繞射特性就應該納入考量。因此，本論文提出了一個結合了「光追跡」與「向量繞射」優點的光學讀取頭模型，不但可以節省計算時間，亦可以達到相當的準確度。

基於先前所提出的光學讀取頭模型，並以DVD+R/RW為例，成功地模擬出其讀取信號(RF signal)、聚焦伺服信號(FES)以及尋軌伺服信號(TES)，並與規格書的標準做比較，以驗證模擬結果的可靠度。此外，本論文也對DVD+R/RW系統，進行公差分析(Tolerance analysis)，其中包含傾斜(Tilt)公差與失焦(Defocus)公差，並與實驗結果作比較，討論公差對於讀出信號及伺服信號的影響。最後，本論文討論了一種在可寫入及可覆寫式系統中常見的現象－饋通現象(Feedthrough)。此現象主要是發生在碟機尋軌時，由於碟片上的溝軌結構(Groove structure)使得聚焦伺服信號會隨著尋軌伺服信號變動的一種干擾(Crosstalk)。此現象會影響聚焦伺服的穩定度，在本論文中會討論其成因以及影響其變化的因素。

可以藉由本論文所提出的光學讀取頭模型的模擬分析，用來在先前設計的步驟當中，發現可能的問題，以期能在發現問題的初步，就能夠找出可能原因，進一步提出解決方案。亦可用於當在碟機系統中發現問題時，將其與以往的模擬結果作比對，以反向推導的方式找出問題可能的原因。

Optical Readout Waveforms Simulation in High Density Optical Storage System

Student: Wei-Liang Kao

Advisor: Chung-Hao Tien

Institute of Electro-Optical Engineering

National Chiao Tung University

Abstract

As the coming of the tera-era, the demand for the storage capacity is increasing. It is known that the storage capacity is governed by the ratio of wavelength (λ) of the laser diode and the numerical aperture (NA) of the objective lens. Therefore, the optical data storage system is developed toward a shorter wavelength and a higher NA. When the NA of the objective lens is higher than 0.6, the vector nature of light will play an important role during readout process. The optical model combined the advantages of the ray-tracing and vector diffraction is proposed to achieve a faster calculation and still maintain the reliability.

Based on the proposed model, the RF signal and servo signals including the focus error signal (FES) and tracking error signals (TES) are demonstrated and successfully verified with the specification under DVD+R/RW system. Moreover, the tolerance analysis of DVD+R/RW system is accomplished. The tilt and defocus effect are simulated and compared with the experimental results to show how the tolerance affect the readout and

servo signals. Finally, this thesis discusses a phenomenon which will happen especially in the recordable and re-writable systems called feedthrough. The feedthrough effect is caused by the groove structures on the recordable disc and lead to a variation in focus error signal with the tracking error signal during track seeking process. The feedthrough effect will deteriorated the performance of the focus servo and the origin and the factors that influence feedthrough are discussed.



Acknowledgement

During my graduate life, I am especially grateful to Professor Chung-Hao Tien, who gave me many valuable advises in research and English presentation skills. Professor Tien provides an excellent environment for me and let me finish my graduate diploma smoothly.

My classmates, Yen-Hsing Lu, Che-Jen Lin, Ming-Jing Chien, Chien-Hsiang Hung and Pi-Ju Cheng, have accompanied me for these two years and made my graduate life colorful and full of joy. The junior classmates, Shih-Wei Ying, Yuan-Jung Yao, Tzu-Hsiang Lan, Shun-Ting Hsiao, and Cho-Chih Chen, also help me a lot in study and bring me a nice memory in my last graduate year. Besides, special thanks to the other classmates in Rm.601 form the warm and happy ambiance for me as well. Moreover, Paul, the French international student, gives me a fresh and nice experience about France. I also want to show my appreciation to Yen-Chih Lee and Wen-Chun Feng, who help me a lot in experiment and give me many useful suggestions about my thesis.

Finally, but essentially, I owe to my parents, grandparents, aunts and my family successful completion of my study. They support me with all their heart to let me complete my study without the fear of disturbance in the rear. Without my family, I could not be what I am today.

Wei-Liang Vic Kao

July, 2006

Table of Contents

Abstract (Chinese) -----	i
Abstract (English) -----	ii
Acknowledgement -----	iv
Table of Contents -----	v
Figure Captions -----	vii
List of Tables -----	xii

Chapter 1 Introduction -----	1
1.1 Motivation-----	1
1.2 Objectives -----	4
1.3 Organization -----	5

Chapter 2 Principles and Literature Review -----	6
2.1 Scalar and Vector Diffraction Theory -----	6
2.1.1 Scalar Diffraction Theory -----	7
2.1.2 Vector Diffraction Theory -----	12
2.1.3 Comparison -----	15
2.2 The Babinet Principle -----	19
2.2.1 Mathematical Formulation and Physical Description -----	19
2.2.2 Generating the Readout, Servo, and Cross-talk -----	22
2.2.3 Applications of the Babinet principle -----	25
2.2.4 Summary -----	27
2.3 Servo mechanisms -----	28
2.3.1 Focus Servo -----	29
2.3.2 Tracking Servo -----	30
2.3.3 Servo Implementation Challenges -----	32
2.4 Summary -----	34

Chapter 3 Simulation Model -----	35
3.1 Simulation Description -----	35
3.1.1 Readout Model -----	38
3.1.2 Parameters -----	39
3.1.3 Simulation Tool -----	40
3.2 System Construction -----	41

3.3 Tolerance Issues -----	45
3.3.1 Tilt Effects -----	45
3.3.2 Defocus Effects -----	47
3.4 Jitter Analysis -----	49
3.5 Summary -----	51
Chapter 4 Simulation Results -----	52
4.1 Results 1 – Readout Waveforms -----	52
4.2 Results 2 – Servo Signals: FES & TES -----	58
4.3 Results 3 – Tolerance Analysis -----	64
4.2.1 Tilt -----	64
4.2.2 Defocus -----	68
4.3 Results 4 – Feedthrough: the crosstalk between TES & FES -----	71
4.4 Summary -----	79
Chapter 5 Conclusion and Future Works -----	80
6.1 Conclusion -----	80
6.2 Future Works -----	82
Reference -----	84

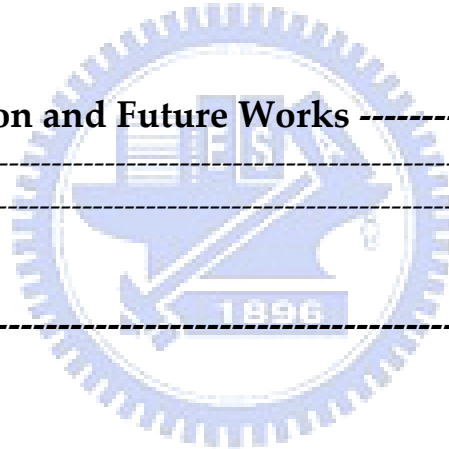


Figure Captions

Chapter 1 Introduction

1.1 Motivation

Fig. 1.1-1 A diagram of the light paths for the CD, DVD and DVR system and electron microscope photographs of the information pits of the three systems ----- 1

Chapter 2 Principles and Literature Review

2.1 Scalar and Vector Diffraction Theory

Fig. 2.1-1 Diffraction geometry ----- 7

Fig. 2.1-2 A linearly polarized beam is brought to focus by a lens ----- 13

Fig. 2.1-3 An x-polarized Gaussian beam is focused by a lens with NA=0.45, and observe the intensity distribution of X-, Y-, and Z-polarization (from the left to the right) on the focal plane. The calculation method is (a) vector diffraction theory, and (b) scalar diffraction theory ----- 16

Fig. 2.1-4 An x-polarized Gaussian beam is focused by a lens with NA=0.85, and observe the intensity distribution of X-, Y-, and Z-polarization (from the left to the right) on the focal plane. The calculation method is (a) vector diffraction theory, and (b) scalar diffraction theory. ----- 17

2.2 The Babinet Principle

Fig. 2.2-1 Light is focused on the disc and formed a reflected field $U_T(x, y)$. The reflected field diffracts to form a field $\tilde{U}_T(x', y')$ at the pupil of the objective lens ----- 19

Fig. 2.2-2 Track layout of the disc ----- 21

Fig. 2.2-3 The Babinet principle used to decompose the signal reflected by the optical disc -----	22
Fig. 2.2-4 Different combinations of the reflection terms generate the servo signal, and two types of crosstalk -----	23

2.3 Servo mechanisms

Fig. 2.3-1 Schematic diagram of pick-up head with focus servo and tracking servo -----	28
Fig. 2.3-2 Astigmatism focus error method -----	29
Fig. 2.3-3 The push-pull tracking method -----	31

Chapter 3 Simulation Model

3.1 Simulation Description

Fig. 3.1-1 The configuration of the simulated DVD system -----	36
Fig. 3.1-2 The unfolded optical path of the simulation model -----	37
(a) The incident optical path	
(b) the reflected optical path.	

Fig. 3.1-3 Schematic diagram of the superposition of the sequential marks -----	38
--	----

3.2 System Construction

Fig. 3.2-1 Transformation from distance to angle -----	41
Fig. 3.2-2 The comparison of simulated results and the specifications of the laser diode -----	42
Fig. 3.2-3 The comparisons of the rim intensities between the simulation and the real case -----	43
Fig. 3.2-4 The focused spot size of the simulation and the real case -----	44

3.3 Tolerance Issues

Fig. 3.3-1 The focused spot with coma aberration of -1λ	45
Fig. 3.3-2 The focused spot with (a) spherical, and (b) defocus aberration	47
Fig. 3.3-3 The relationship between the FES and the plot of Jitter vs. Defocus --	48

3.4 Jitter Analysis

Fig. 3.4-1 Time interval analysis and the definition of jitter	49
Fig. 3.4-2 Window occupation method	50

Chapter 4 Simulation Results

4.1 Results 1 – Readout Waveforms

Fig. 4.1-1 The readout signals of the isolated marks from 3T to 14T (without 12T & 13T)	53
Fig. 4.1-2 The simulation result of the readout signal (eyepattern)	54
Fig. 4.1-3 The real case of the readout signal (eyepattern)	55
Fig. 4.1-4 Readout signals from spaces and marks	55

4.2 Results 2 – Servo Signals: FES & TES

Fig. 4.2-1 The astigmatism method and the intensity distributions at position --	59
(a) M (too-near)	
(b) P (in-focus)	
(c) N (too-far)	
Fig. 4.2-2 The comparison of the FES between the simulation result and the real case	60
Fig. 4.2-3 The relationship between the FES and the sum signal on the photo-detector	62
(a) the simulation result	
(b) the signals from oscillator	

4.3 Results 3 – Tolerance Analysis

Fig. 4.3-1 The RF signal with radial tilt of 1.5°	64
Fig. 4.3-2 The tilt effect upon the RF signal with different tilt angles	65
(a) 0°	
(b) $10'$	
(c) $20'$	
(d) $30'$	
Fig. 4.3-3 The relationship between the radial tilt and the jitter value and the RF amplitude	66
Fig. 4.3-4 The influence of the radial and tangential tilt on the jitter (DVD+R disc)	67
Fig. 4.3-5 The linear range of the FES and the three cross-sections of the intensity distributions at A. too-near, B. in-focus, and C. too-far positions	68
Fig. 4.3-6 The simulated jitter value as a function of the defocus distance	70
Fig. 4.3-7 The experimental jitter value as a function of the defocus distance ---	70

4.4 Results 4 – The Crosstalk between FES & TES: Feedthrough

Fig. 4.4-1 The astigmatism focus servo method and the layout of the track direction and photo-detector	71
Fig. 4.4-2 The diffraction of the incident wave by the groove structure on the disc	72
Fig. 4.4-3 The FES and TES of the ideal ODS system with an aberration-free objective lens	73
Fig. 4.4-4 The FES and TES of the ODS system with an objective lens of 0.25λ coma aberration	75
Fig. 4.4-5 The FES and TES of the ODS system with an objective lens of 0.25λ astigmatism aberration	76
Fig. 4.4-6 The comparison of the false FES (feedthrough) with different conditions	76
Fig. 4.4-7 The simulated intensity distributions and the contour plots on the photo-detector	77
(a) the ideal case	
(b) at the land center	
(c) at the groove center	

Chapter 5 Conclusion and Future Works

5.2 Future Works

Fig. 5.2-1 Blu-ray disc technology ----- 82



List of Tables

Chapter 2

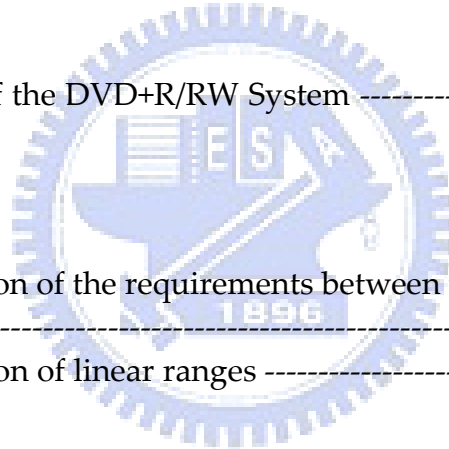
Table 2.1 The polarization of the emergent beam is E_1 , and the original polarization is E_0 under the assumption of lossless refraction -----	14
Table 2.2 Maximum intensities along x-, y-, and z-direction and their comparisons -----	18
Table 2.3 The diffraction terms resulting from the Babinet decomposition -----	25
Table 2.4 The relationships between the different disc formats and the tracking schemes -----	32

Chapter 3

Table 3.1 Parameters of the DVD+R/RW System -----	39
--	----

Chapter 4

Table 4.1 The comparison of the requirements between real and simulation results -----	56
Table 4.2 The comparison of linear ranges -----	61



Chapter 1

Introduction

1.1 Motivation

As the coming of the tera-era, the demand of the recording capacity is increasing. The areal density is governed by the numerical aperture (NA) and the wavelength (λ) of the optical pick-up head (PUH). An optical data storage (ODS) system is developed toward a shorter wavelength laser diode and a higher numerical aperture objective lens, where the focused spot diameter is proportional to λ/NA , to achieve a higher areal density, as shown in Fig. 1.1-1.

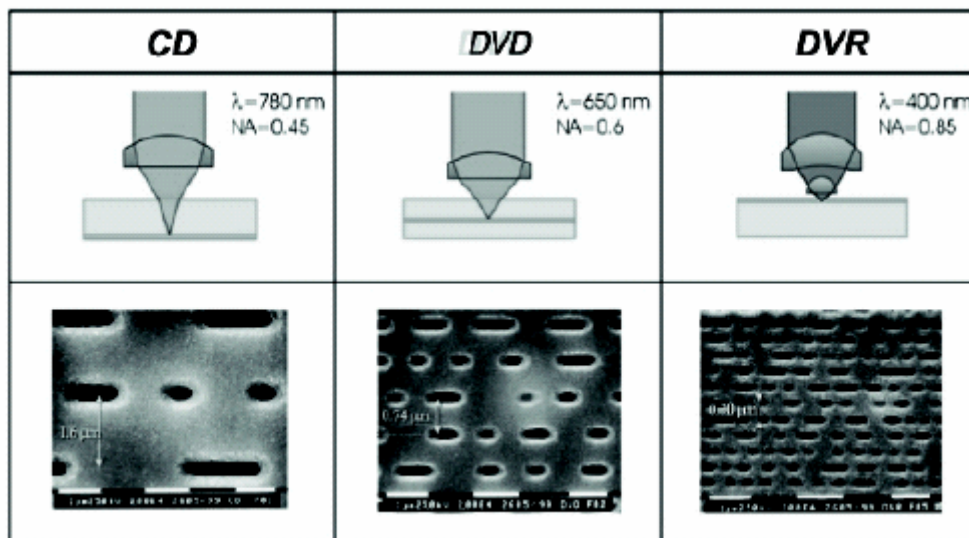


Fig. 1.1-1 A diagram of the light paths for the CD, DVD and DVR system and electron microscope photographs of the information pits of the three systems^[1]

The optics of the ODS system including the fundamental principles of each optical component, disk recording are introduced in many literatures.

^{[2][3][4]} These theories describe the propagation of the light in the optical pick-up head, the interaction between the light and the media and the extraction of the readout and servo signals from the photo-detectors. The literatures in this field primarily based on the geometry optics and the scalar diffraction theory proven to successfully characterize most of the observed phenomena.

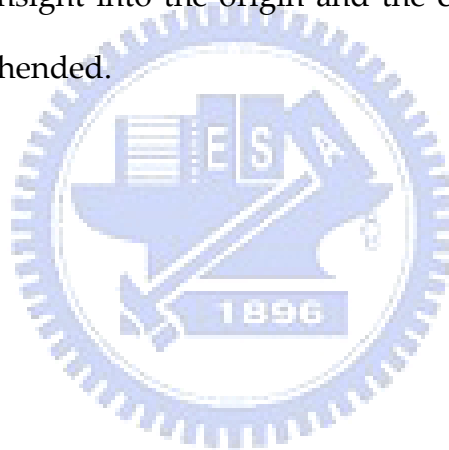
When NA of the objective lens is higher than 0.6, the vector nature of the light field plays an important role in the optical readout process. The vector diffraction is needed to accurately model the interaction between the polarized light and the storage media. Because the calculation of the model based on vector diffraction theory is concerning with the interaction between the polarization of the light and the optical components, the cost of such model is extensive computation resources, such as the long computing time and the large memory capacity. Notwithstanding, to attaining acceptable levels of performance and reliability in the oncoming high-NA optical data storage system, the simulation model based on the vector diffraction theory is indispensable and has been proposed by many research groups.^[5]

The compromising method is combining the ray-tracing and the vector diffraction model. The beam is traced through the entrance pupil of the ODS system, the objective lens, working distance and the disc substrate to the focal point. Near the focus the rays are transformed to the diffraction calculation. After reflected from the disc, the beam propagates a distance to a region where the ray-tracing is valid once again.

A typical method to model the diffraction effect from the optical disc is to use a mark structure described by the Fourier series expansion in two

dimensions or by the fast Fourier transform algorithm. These methods can accurately estimate the optical phenomena in the optical data storage system, but have a less insight into the physics of the signal generation.

A different method called the Babinet principle which is based on the decomposition of the returning beam from a simplified disc structure is introduced to provide a physical insight into the diffraction mechanism of the optical readout system.^[6] The Babinet principle is adopted in the proposed model to decompose the reflected light from the information layer of the disc into separate components that compose of the data signal, servo signals, and crosstalk so that the insight into the origin and the characteristics of various signals can be comprehended.

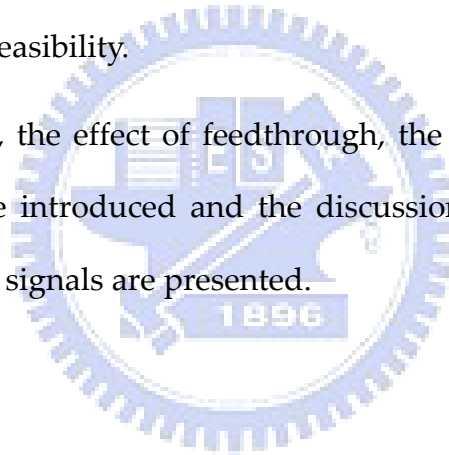


1.2 Objectives

Based on the Babinet principle and the vector diffraction theory, the objectives of this thesis are to simulate the readout signal and the servo signals including focus-error signal (FES) and tracking-error signal (TES) in the first stage. These signals are quantitatively compared with the specification requirements to verify the validity of the results.

In the following stage, the tolerance analysis including tilt and defocus of the key components are analyzed. Furthermore, tolerance experiments based on the DVD-system will be implemented to verify the proposed model and demonstrate the feasibility.

In the final stage, the effect of feedthrough, the interaction between the two servo signals, are introduced and the discussion of the causes and the influence on the servo signals are presented.



1.3 Organization of This Dissertation

This thesis is organized as following: the basic principles and the prior studies utilized for constructing the model is reviewed in **Chapter 2**. In **Chapter 3**, the simulation model and system configuration are proposed and described. The simulation results including the readout signal, the servo signals, the tolerance analysis, and the effect of feedthrough is demonstrated and discussed in **Chapter 4**. The conclusion and the future works are given in **Chapter 5**.



Chapter 2

Principles and Literature Review

In **Chapter 2**, the theories of the scalar and vector diffraction in the optical data storage system and the preliminary principles of decomposing the light reflected from the disc structure are reviewed; moreover, the fundamentals of the servo mechanism is described at the end of **Chapter 2**.

2.1 Scalar and Vector Diffraction Theory

Scalar diffraction theory is employed in the analysis, when the following two conditions are satisfied: (1) the NA is lower than 0.6; (2) the size of details on the disc are larger than the magnitude of the light wavelength (λ) employed. Because the bending of the rays by the focusing element is fairly small, the electromagnetic fields before and after the element to have a more or less the same orientations. However, when the optical system with a severe bending of the light rays, such as a high-NA system, is adopted, the polarization effects of the light should be significant. The applicability of the scalar diffraction theory is based on the easy evaluation by the method of stationary phase approximation. In the stationary phase approximation, the plane wave spectrum of the convergent beam at the exit pupil is equivalent to the light amplitude distribution at that pupil; therefore, each geometric ray represents one plane wave of the spectrum.

2.1.1 Scalar Diffraction Theory ^[7]

The Huygens-Fresnel principle can be written

$$U(x, y) = \frac{z}{j\lambda} \iint_{\Sigma} U(\xi, \eta) \frac{e^{jk r_{01}}}{r_{01}^2} d\xi d\eta \quad (2.1-1)$$

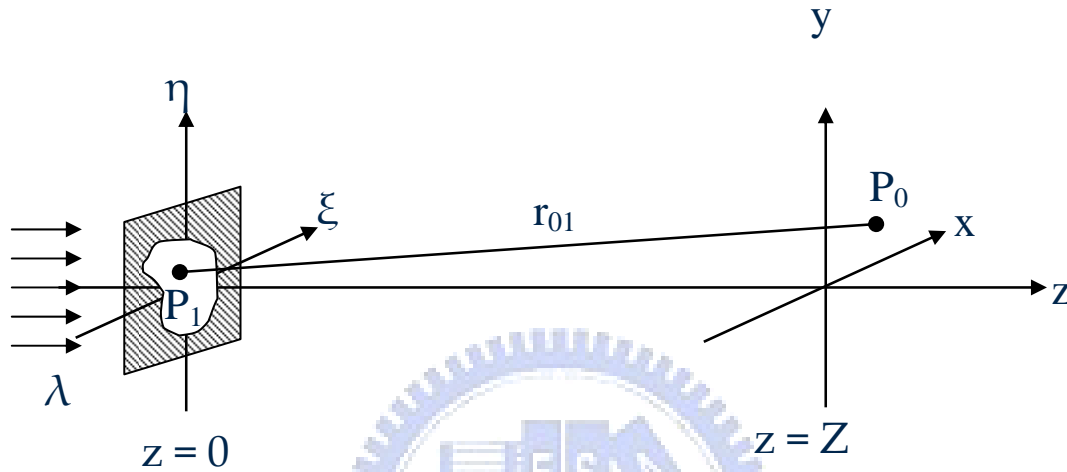


Fig. 2.1-1 Diffraction geometry

where the distance r_{01} is given by $r_{01} = \sqrt{(x-\xi)^2 + (y-\eta)^2 + z^2}$. As shown in Fig. 2.2-1, the diffraction aperture lies in the (ξ, η) plane, and is illuminated in the positive z direction. By the paraxial assumptions, (2.1-1) becomes

$$U(x, y) = \frac{e^{jkz}}{j\lambda z} \iint_{-\infty}^{\infty} U(\xi, \eta) e^{j \frac{\pi}{\lambda z} [(x-\xi)^2 + (y-\eta)^2]} d\xi d\eta \quad (2.1-1)$$

and another form of (2.1-1) is

$$U(x, y) = \frac{e^{jkz}}{j\lambda z} e^{j \frac{\pi}{\lambda z} (x^2 + y^2)} \iint_{-\infty}^{\infty} \left[U(\xi, \eta) e^{j \frac{\pi}{\lambda z} (\xi^2 + \eta^2)} \right] e^{-j \frac{2\pi}{\lambda z} (x\xi + y\eta)} d\xi d\eta \quad (2.1-2)$$

which is the Fourier transform of the product of the complex field and a quadratic phase term. (2.1-1) and (2.1-2) is the Fresnel diffraction (Near field) integral. If the phase term in the brackets of (2.1-1) approaches unity, i.e.

$$e^{j \frac{\pi}{\lambda z} (\xi^2 + \eta^2)} \approx 1 \Rightarrow \frac{\pi}{\lambda z} (\xi^2 + \eta^2)_{\max} \ll 1 \text{ or } z \gg \frac{D^2}{\lambda}$$

where the D represents the maximum dimension of the aperture, the observed field is the Fourier transform of the aperture.

$$U(x, y) = \frac{e^{jkz}}{j\lambda z} e^{j \frac{\pi}{\lambda z} (x^2 + y^2)} \int \int_{-\infty}^{\infty} U(\xi, \eta) e^{-j \frac{2\pi}{\lambda z} (x\xi + y\eta)} d\xi d\eta \quad (2.1-3)$$

This is the Fraunhofer (Far field) diffraction integral where $u = \frac{x}{\lambda z}$, $v = \frac{y}{\lambda z}$.

Except the phase factor preceding the integral, this expression is simply the Fourier transform of the aperture.

$$U(x, y) = C * F \{U(\xi, \eta)\} \Big|_{u=\frac{x}{\lambda z}, v=\frac{y}{\lambda z}} \quad (2.1-4)$$

where $C = \frac{e^{jkz}}{j\lambda z} e^{j \frac{\pi}{\lambda z} (x^2 + y^2)}$ and F represents the Fourier transform operation.

There is an analogue method to determine the diffraction patterns after propagating through a distance called the angular spectrum of plane waves. Any complex amplitude distribution of the light can be decomposed into a spectrum of plane waves. The plane waves travel in different directions across the system, and then are superimposed to form a diffraction pattern at the destination plane.

In the ODS system, the light source is the laser diode which has a Gaussian complex amplitude distribution. The following of this section try to use this amplitude distribution to derive the diffraction formulas and compare this to the aforementioned theory. Generally, the Gaussian beam propagates along the z-axis has the following complex amplitude distribution:

$$U(x, y) = U_0 \exp(-\alpha x^2 - \beta y^2) \quad (2.1-5)$$

In (2.1-5), α and β are complex numbers. Consider the Fourier transform and corresponding inverse Fourier transform of such amplitude distribution at the $z = 0$ plane:

$$F\{U(x, y, 0)\} = \int_{-\infty}^{\infty} \int_{-\infty}^{\infty} U(x, y, 0) \exp[-j2\pi(xu + yv)] dx dy \quad (2.1-6)$$

$$U(x, y, 0) = \int_{-\infty}^{\infty} \int_{-\infty}^{\infty} F\{U(x, y, 0)\} \exp[j2\pi(xu + yv)] du dv \quad (2.1-7)$$

The right side of (2.1-7) is the superposition of plane waves propagating long the unit vector σ , where

$$\sigma = u \hat{x} + v \hat{y} + \sqrt{1 - u^2 - v^2} \hat{z} \quad (2.1-8)$$

* The evaluation of the integral:

$$\int_{-\infty}^{\infty} \int_{-\infty}^{\infty} U(x, y, 0) \exp[-j2\pi(xu + yv)] dx dy = \frac{\pi U_0}{\sqrt{\alpha\beta}} \exp\left[-\pi^2 \left(\frac{u^2}{\alpha} + \frac{v^2}{\beta}\right)\right]$$

The amplitude of the propagating plane wave are the Fourier transform of the $U(x, y)$ with the frequency (u, v) . The plane waves propagate along the z -axis from the origin to the $z=Z$ plane, and the resulting distribution at the $z=Z$ plane is obtained by the superposition of these plane waves after traveling a Z distance.

$$U(x, y, Z) = \int_{-\infty}^{\infty} \int_{-\infty}^{\infty} F\{U(x, y, 0)\} \exp\left\{j2\pi\left[xu + yv + Z\sqrt{1-u^2-v^2}\right]\right\} dudv \quad (2.1-9)$$

A method called stationary-phase approximation can be utilized to evaluate the integral value of (2.1-9).^{[7][8]} Consider a two-dimensional integral

$$I = \iint f(\xi, \eta) \exp[j\kappa\phi(x, y)] d\xi d\eta \quad (2.1-10)$$

where $f(\xi, \eta)$ is a complex function, and $\phi(\xi, \eta)$ is a real function, and κ is a large real number, and the domain of the integration is a subset of the $\xi\eta$ -plane. The small variation of the function $\phi(\xi, \eta)$ will be amplified by the large real number κ , and result in the rapid oscillation of the phase term. On the other hand, the complex function $f(\xi, \eta)$ is a slow variation function which has a negligible effect on the integral. The main contribution of this integral is from the regions in the neighborhood of the stationary point of $\phi(\xi, \eta)$ which is defined as (2.1-11)

$$\frac{\partial}{\partial x} \phi(\xi_0, \eta_0) = \frac{\partial}{\partial y} \phi(\xi_0, \eta_0) = 0 \quad (2.1-11)$$

The integral in (2.1-10) can be approximated as

$$\begin{aligned} I &= \iint f(\xi, \eta) \exp[j\kappa\phi(\xi, \eta)] d\xi d\eta \\ &\cong \frac{j2\pi\nu}{\kappa\sqrt{\alpha\beta - \gamma^2}} f(\xi_0, \eta_0) \exp[j\kappa\phi(\xi_0, \eta_0)] \end{aligned} \quad (2.1-12)$$

$$\text{where } \alpha = \frac{\partial^2 \phi}{\partial \xi^2} \quad \beta = \frac{\partial^2 \phi}{\partial \eta^2} \quad \gamma = \frac{\partial^2 \phi}{\partial \xi \partial \eta} \quad \nu = \begin{cases} 1, & \alpha\beta > \gamma^2, \alpha > 0 \\ -1, & \alpha\beta > \gamma^2, \alpha < 0 \\ -j, & \alpha\beta < \gamma^2 \end{cases} \quad (2.1-13)$$

When the real function $\phi(\xi, \eta)$ has the form

$$\phi(\xi, \eta) = \sqrt{1 - \xi^2 - \eta^2} + A\xi + B\eta \quad (2.1-14)$$

where A and B are real numbers. The integral in (2.1-10) can be approximated as follow:

$$\begin{aligned} I &= \iint f(\xi, \eta) \exp\left[j\kappa(\sqrt{1 - \xi^2 - \eta^2} + A\xi + B\eta)\right] d\xi d\eta \\ &\cong \frac{-j2\pi}{\kappa} f_s(A, B) \exp\left[j\kappa\sqrt{1 - A^2 - B^2}\right] \end{aligned} \quad (2.1-15)$$

$$f_s(A, B) = \frac{f\left(\frac{A}{\sqrt{1 + A^2 + B^2}}, \frac{B}{\sqrt{1 + A^2 + B^2}}\right)}{1 + A^2 + B^2} \quad (2.1-16)$$

where $f_s(A, B)$ is a stretch version of $f(\xi, \eta)$. Comparison of (2.1-9) with (2.1-15) shows that the two integrals are identical supposed that one makes the following associations:

$$f(u, v) \rightarrow F\{U(x, y, z=0)\} ; \kappa = 2\pi z ; A = \frac{\xi}{Z} ; B = \frac{\eta}{Z}$$

Consequently, the integral in (2.1-9) is an approximated form by the stationary-phase method as (2.1-16):

$$U(x, y, Z) \cong \frac{-j}{Z} \exp\left[j2\pi\sqrt{x^2 + y^2 + Z^2}\right] F_s\left\{U(x, y, z=0)\right\}_{\substack{A=\frac{\xi}{Z} \\ B=\frac{\eta}{Z}}} \quad (2.1-17)$$

This is the fundamental equation of the scalar diffraction theory in the far-field regime. The exponential term in (2.1-17) is the curvature phase representing a radius of curvature Z . The stretching operation must be put on the function before Fourier transformation. Comparison of the approximated result (2.1-17) with the far-field integral (2.1-3) demonstrates the consistency.

2.1.2 Vector Diffraction Theory ^{[3][4]}

The simple treatment of the effects concerning the polarization will be introduced in this section. Replacing the rigorous solution of the Maxwell's equations with the physical phenomenon of bending of the plane wave by high-NA lens is an intuitive approach about the propagation of the electromagnetic waves.

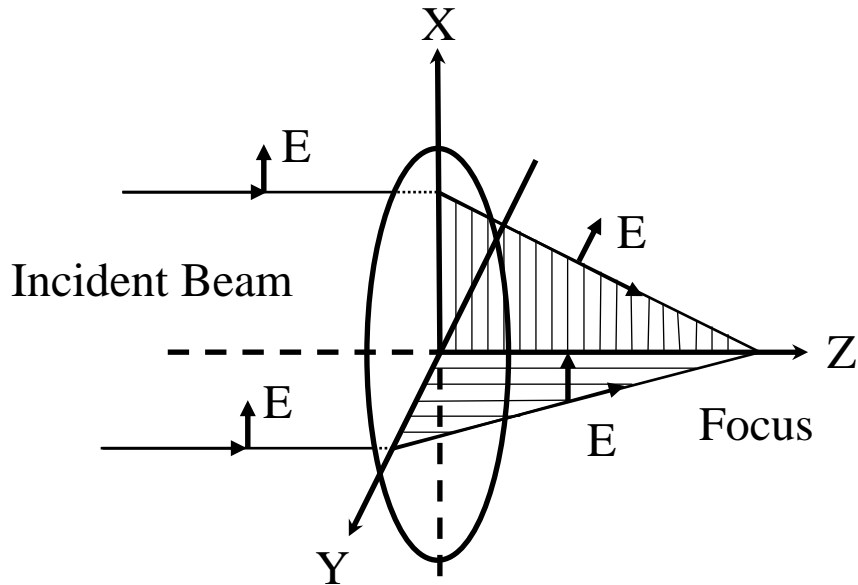


Fig. 2.1-2 A linearly polarized beam is brought to focus by a lens. The E-field is the electric field indicating the direction of the polarization.

Consider a linearly polarized beam propagates along the z direction, as shown in Fig. 2.1-2. The incident direction of propagation is $\sigma_0 = (0,0,1)$, and the corresponding direction of propagation after the lens is $\sigma_1 = (\sigma_x, \sigma_y, \sigma_z)$.

The incident polarization electric $E_0 = (1,0,0)$ can be decomposed into two components, s-polarization and p-polarization. The s-polarization is in the plane of the σ_0 and σ_1 , and remains in the same direction of incidence after passing through the lens. In the meanwhile, the p-polarization reorients to the perpendicular direction of the emergent rays. If the refraction process is lossless, the simple geometry is used to determine the new emerging polarization. Given the direction of incident beam σ_0 and the direction of the emergent beam σ_1 , the polarization of the emergent beam can be resolved with the arbitrary polarization state of the incident beam, as listed in Table 2.1.

A similar calculation can be derived in the same procedure from an incident beam with polarization along y-axis.

Table 2.1 The polarization of the emergent beam is E_1 , and the original polarization is E_0 under the assumption of lossless refraction.

Incident polarization	Emerging polarization
$\sigma_0 = (0,0,1)$	$\sigma_1 = (\sigma_x, \sigma_y, \sigma_z)$
$E_0 = (1,0,0)$	$E_1 = \left[1 - \frac{\sigma_x^2}{1 + \sigma_z}, \frac{-\sigma_x \sigma_y}{1 + \sigma_z}, -\sigma_x \right]$
$E_0 = (0,1,0)$	$E_1 = \left[\frac{-\sigma_x \sigma_y}{1 + \sigma_z}, 1 - \frac{\sigma_y^2}{1 + \sigma_z}, -\sigma_y \right]$

Note that the beam cross-section changes after refraction in consequence of plane wave refraction. The cross-section propagate along σ_1 is reduced by a factor σ_z , and therefore, its amplitude is increased by a factor $1/\sigma_z$. The correct emerging polarization amplitude is E_1/σ_z .

According to (2.1-17), the amplitude distribution is Fourier-analyzed across any plane, and the various spatial Fourier components can be identified as plane waves traveling in different directions. The amplitude at any point can be determined by superposing the constituent plane waves to join the phase shift obtained during propagation. Incorporating the polarization state of Table 2.1 with (2.1-17) to get the formula for vector diffraction:

$$\begin{pmatrix} U_x(x, y, z) \\ U_y(x, y, z) \\ U_z(x, y, z) \end{pmatrix} = \iint \frac{1}{\sqrt{\sigma_z}} \begin{pmatrix} 1 - \frac{\sigma_x^2}{1 + \sigma_z} & -\frac{\sigma_x \sigma_y}{1 + \sigma_z} \\ -\frac{\sigma_x \sigma_y}{1 + \sigma_z} & 1 - \frac{\sigma_y^2}{1 + \sigma_z} \\ -\sigma_x & -\sigma_y \end{pmatrix} \times \begin{pmatrix} F\{U_x(x, y, z=0)\} \\ F\{U_y(x, y, z=0)\} \end{pmatrix} \exp[j2\pi(x\sigma_x + y\sigma_y + z\sigma_z)] d\sigma_x d\sigma_y \quad (2.1-18)$$

and (2.1-18) is the vector version of (2.1-17)

2.1.3 Comparison

The simplest focusing theorem is based on the scalar diffraction and the paraxial approximation. This simplest theorem is applicable only when the numerical aperture of the lens is low/moderate. When the NA of the lens up to the scale of which the polarization effect can not be neglect, the focusing problem should be dealt with the vector diffraction theory.

In this section, the author try to demonstrate the objective lens with different NA (NA=0.45, 0.85) to observe the intensity distributions in different polarization directions on its focal plane. The light is an x-polarized Gaussian beam, and is incident to the lens with NA of 0.45 (CD) or 0.85 (DVR). The aforementioned vector and scalar diffraction theory are employed.

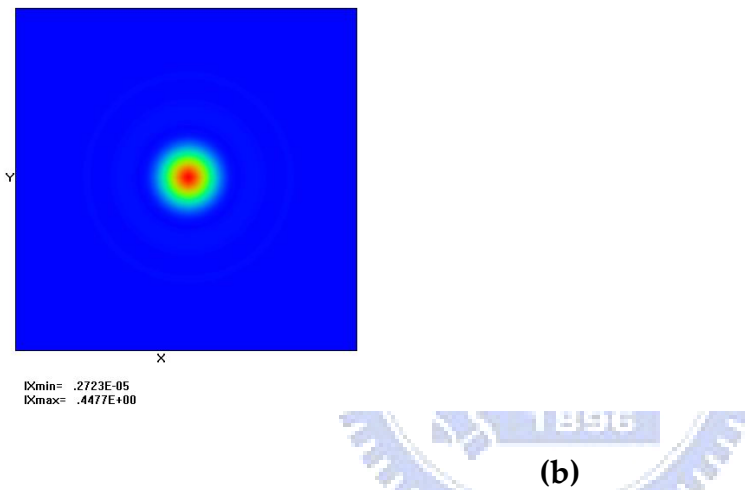
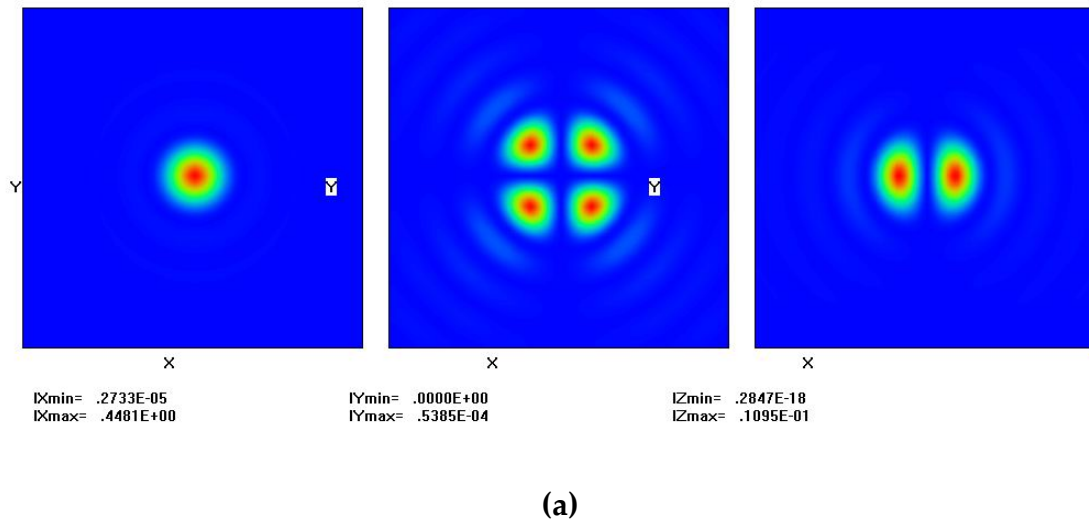


Fig. 2.1-3 An x-polarized Gaussian beam is focused by a lens with $NA = 0.45$, and observe the intensity distribution of X-, Y-, and Z-polarization (from the left to the right) on the focal plane. The calculation method is (a) vector diffraction theory, and (b) scalar diffraction theory.

The x- and y-axis in Fig. 2.1-3 and Fig. 2.1-4 are the coordinates in the focal plane and range from -5λ to 5λ . The intensity distributions in Fig. 2.1-3(a) and Fig. 2.1-4(s) are X-, Y-, and Z polarizations. There is only one plot in Fig. 2.1-3(b) and Fig. 2.1-4(b) because the scalar diffraction theory does not take polarizations into consideration.

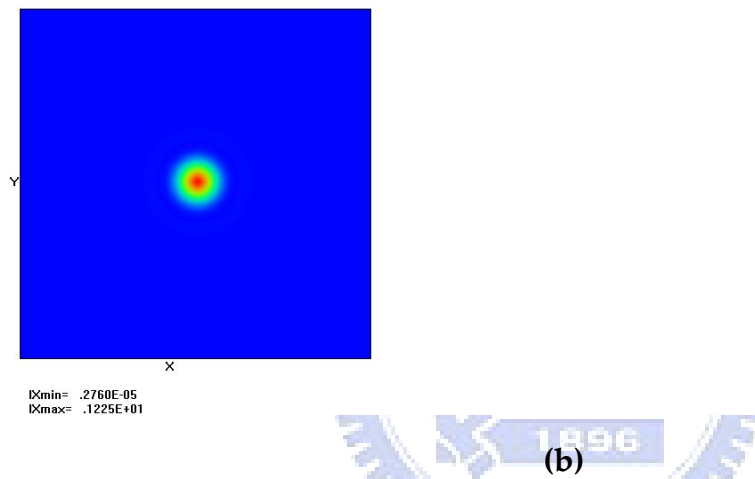
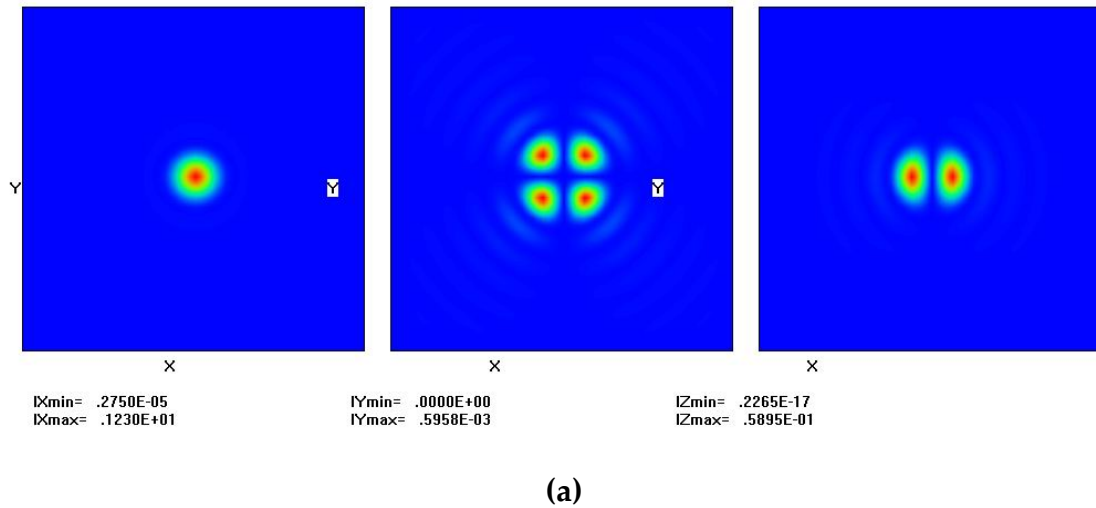


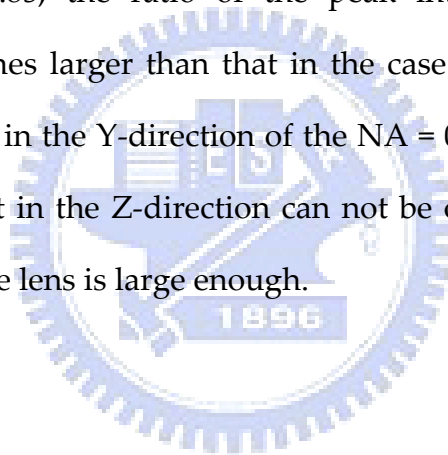
Fig. 2.1-4 An x-polarized Gaussian beam is focused by a lens with $NA = 0.85$, and observe the intensity distribution of X-, Y-, and Z-polarization (from the left to the right) on the focal plane. The calculation method is (a) vector diffraction theory, and (b) scalar diffraction theory.

As shown in Fig. 2.1-3(a) and 2.1-4(a), in y-polarization four peaks occur near the focus, and in the z-direction two peaks appear under the vector diffraction calculation. The summary of the maximum intensities along each direction and their comparisons are shown in Table 2.2.

Table 2.2 Maximum intensities along x-, y-, and z-direction and their comparisons

VECTOR					
NA	X (a.u.)	Y (a.u.)	Z (a.u.)	Y/X (%)	Z/X (%)
0.45 (CD)	0.4481	0.0000539	0.01095	0.01%	2.44%
0.85 (DVR)	1.2300	0.0005958	0.05895	0.05%	4.79%

In the case of NA = 0.45, the ratio of the peak intensity between Y and X-direction is 0.01% which can be neglected and so does that of NA = 0.85. For the case of NA = 0.85, the ratio of the peak intensity between Z and X-direction is 1.96 times larger than that in the case of NA=0.45 and is 95.8 times larger than that in the Y-direction of the NA = 0.85. For this reason, the diffraction component in the Z-direction can not be omitted any more while the NA of the objective lens is large enough.



2.2 The Babinet Principle ^{[5][9]}

The traditional way to model the propagation and interaction of the light in the ODS system is use a Hopkins-type method in which the mark structure is expressed by the Fourier series expansion.^[2] This model has a good estimate of the light, but has a less comprehension about the physics of the signal generation. The Babinet principle can provide quantitative results of the diffraction mechanism by decomposing the reflected field from the recording layer of the disc into ingredient components; these components with different combination form the readout signal, servo signals, and the crosstalk, respectively.

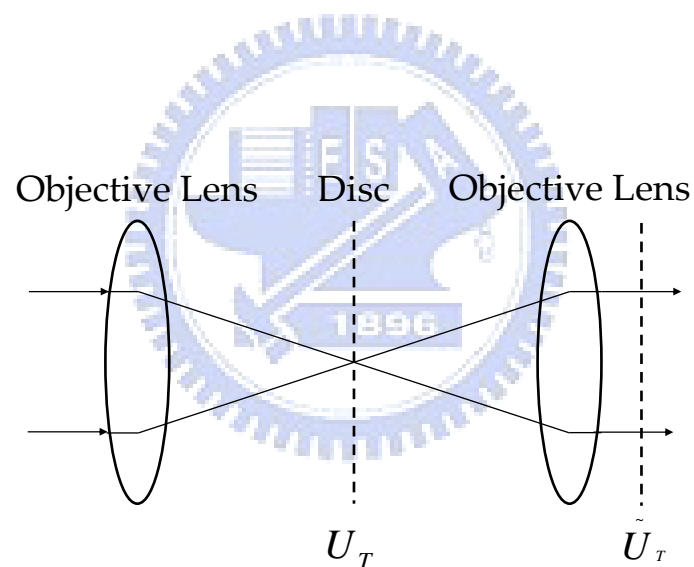


Fig. 2.2-1 Light is focused on the disc and formed a reflected field $U_T(x, y)$.

The reflected field diffracts to form a field $\tilde{U}_T(x', y')$ at the pupil of the objective lens.

2.2.1 Mathematical Formulations and Physical Description

Consider a model which the objective lens focus the incident light onto the

recording layer of the optical disc and the light is recollimated by the objective lens, accordingly, as shown in Fig. 2.2-1. The total light field reflected from the disk is $U_T(x, y)$, where the x and y represent the coordinates in the plane of the recording layer. The reflected beam is collimated by the objective lens and form a light field $\tilde{U}_T(x', y')$ at the exit pupil of the objective lens, where the x' and y' represent the coordinates at the pupil.

The Babinet principle assumes that the total field reflected from the recording layer is the summation of the fields reflected from the separate regions.

$$U_T = \sum_{i=1}^{i=N} U_i \quad (2.2-1)$$

U_i are the non-overlapping composing regions on the optical disc. The summation of N components cover entire domain of $U_T(x, y)$. Linear operations performed on $U_T(x, y)$ is a summation of the linear operation of each component U_i .

$$\tilde{U}_T = \sum_{i=1}^{i=N} \tilde{U}_i \quad (2.2-2)$$

The tilde refers to the linear operation of the propagation from the disc plane to the exit pupil of the objective lens.

The separate components correspond to the light field reflected from

different marks of two adjacent tracks, T1 and T2, as depicted in Fig. 2.2-2. The laser spot focused on the recording layer scans over track T1 with an offset Δy . The marks on T1 and T2 are denoted as M1 and M2, respectively. The track pitch is indicated by P.

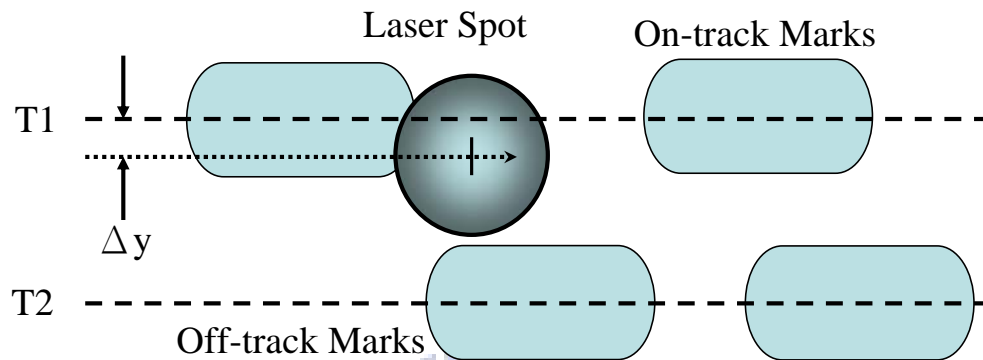


Fig. 2.2-2 Track layout of the disc

Each component of U_i include the three parts: (1) the electric field reflected from mark M1 of track T1, U_{M1} ; (2) the electric field reflected from mark M2 of track T2, U_{M2} ; (3) the electric field reflected from the land, U_i . The Babinet principle declare the total reflection from the recording layer U_T as

$$U_T = r_L U_F + (r_M - r_L)(U_{M1} + U_{M2}) \quad (2.2-3)$$

where the r_L and r_M are the complex reflectance of the land and the mark, respectively, and U_F is the reflection form the flat surface of the disc, as illustrated in Fig. 2.2-3.

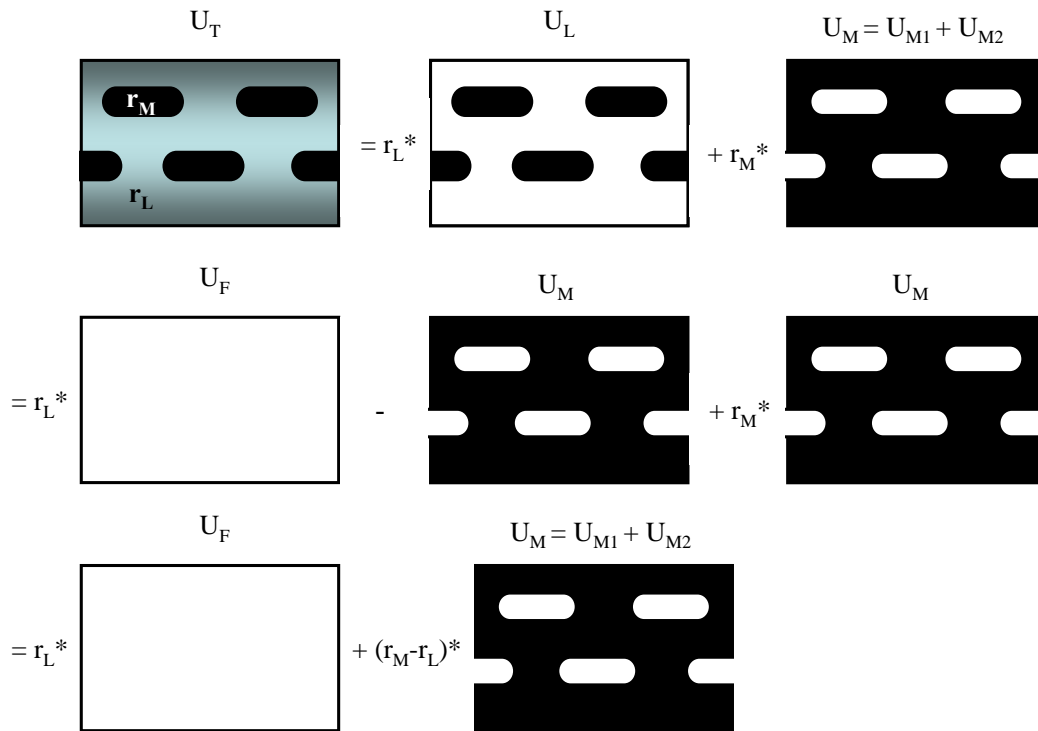


Fig. 2.2-3 The Babinet principle used to decompose the signal reflected by the optical disc

The ingredients U_{M1} and U_{M2} are binary value with a maximum of one and a minimum of zero. Take the groove structure into account, the flat reflection term, U_F transform to the form $U_F = \exp[i\phi(x, y)]$, where the $\phi(x, y)$ represents the phase imported by the grooves as a function of the position on the recording layer.

2.2.2 Generating the Readout, Servo, and Crosstalk

The total field at the exit pupil of the objective lens, \tilde{U}_T , propagate to the detector that generate the data signal and the servo signals. The data signal reveals the mark distribution beneath the scanning laser spot; the servo signal

is sensible to the offset Δy . The crosstalk between the data channels is caused by the interaction between the rim of the focused laser spot and the adjacent tracks. The reflection from the on-track mark, \tilde{U}_{M1} , are important factor for analysis. \tilde{U}_{M1} shows the symmetry in the amplitude and the phase along the track direction when the laser spot scans over the mark M1.

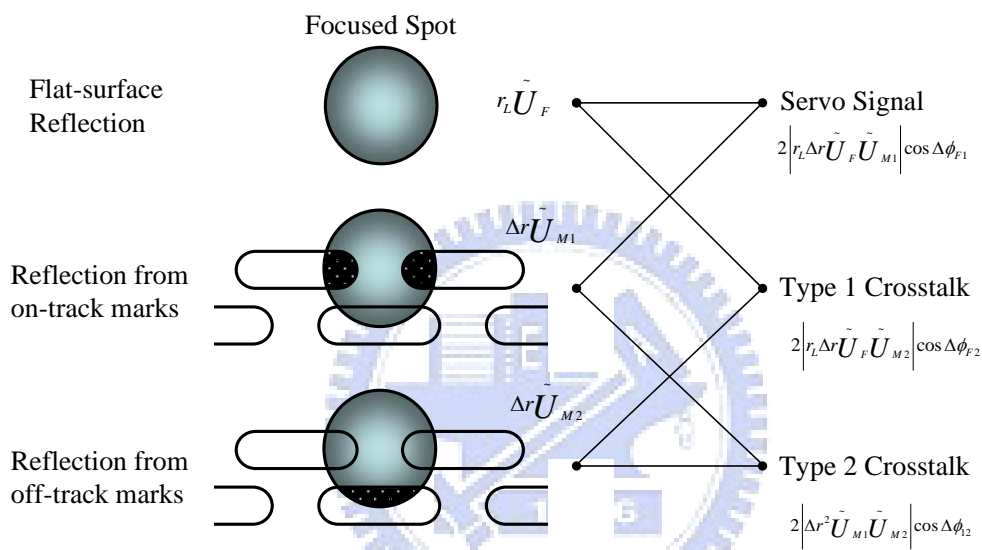


Fig. 2.2-4 Different combinations of the reflection terms generate the servo signal, and two types of crosstalks

The amplitude diffraction pattern splits and the phase of the amplitude diffraction pattern rotates when the laser spot scans over an on-track mark. The rotation of the phase is due to the linear phase term has been introduced into the reflection field during scanning the off-track marks. The component fields, \tilde{U}_F , \tilde{U}_{M1} , and \tilde{U}_{M2} with different combinations form the data signal, servo signals, and crosstalks, as illustrated in Fig. 2.2-4.

Three kinds of signals are illustrated in Fig. 2.2-4; firstly, the diffraction

from the flat reflection, $r_L \tilde{U}_F$, combines with the diffraction from the on-track mark, $\Delta r \tilde{U}_F$, to form the servo signal:

$$2 \left| r_L \Delta r \tilde{U}_F \tilde{U}_{M1} \right| \cos \Delta \phi_{F1} \quad (2.2-4)$$

where $\Delta r = r_M - r_L$ and $\Delta \phi_{F1}$ is the phase difference between the two constructed components. Secondly, the type one crosstalk:

$$2 \left| r_L \Delta r \tilde{U}_F \tilde{U}_{M2} \right| \cos \Delta \phi_{F2} \quad (2.2-5)$$

, is formed by the flat reflection and the diffraction from the off-track marks. Lastly, the diffraction from the on-track and the off-track mark lead to a type two crosstalk:

$$2 \left| \Delta r^2 \tilde{U}_{M1} \tilde{U}_{M2} \right| \cos \Delta \phi_{12} \quad (2.2-6)$$

A summary of the terms generated by the different combinations of the diffraction terms and its physical explanation is listed in Table 2.3. The detector responds to the irradiance of the light field, $\tilde{I}_T \propto \left| \tilde{U}_T \right|^2$. The servo current is formed by integrating the irradiance of the resulting diffraction term:

$$I_{SERVO} = \int_{\Omega} 2 \left| r_L \Delta r \tilde{U}_F \tilde{U}_{M1} \right| \cos \Delta \phi_{F1} dx' dy' \quad (2.2-7)$$

where Ω is the area of the pupil aperture. The data signal is determined by the same way:

$$I_{DATA} = \int_{\Omega} \left| \Delta r \tilde{U}_{M1} \right|^2 dx' dy' \quad (2.2-8)$$

Table 2.3 The diffraction terms resulting from the Babinet decomposition ^[5]

Diffraction Terms	Formula	Physical Description
Background	$\left r_L \tilde{U}_F \right ^2$	Background reflection
Data Signal	$\left \Delta r \tilde{U}_{M1} \right ^2$	Interference of the M1 with itself
Type 0 crosstalk	$\left \Delta r \tilde{U}_{M2} \right ^2$	Interference of the M2 with itself
Servo Signal	$2 \left r_L \Delta r \tilde{U}_F \tilde{U}_{M1} \right \cos \Delta \phi_{F1}$	Interference of the M1 with background
Type 1 crosstalk	$2 \left r_L \Delta r \tilde{U}_F \tilde{U}_{M2} \right \cos \Delta \phi_{F2}$	Interference of the M2 with background
Type 2 crosstalk	$2 \left \Delta r^2 \tilde{U}_{M1} \tilde{U}_{M2} \right \cos \Delta \phi_{12}$	Interference of the M1 and the M2

2.2.3 Applications of the Babinet principle

In this section, the two applications of the Babinet principle is introduced. The first application is the explanation of the origin of the differential phase detection (DPD) method, which is used as a tracking method to maintain the laser spot on the target track. The DPD tracking signal originates from the rotation of the diffraction pattern which been detected by the quadrants of the detector.

Case I: $r_L \neq 0, r_M = 0$, without grooves and one isolated mark, M1

The returning irradiance pattern is

$$\tilde{I}_T \propto \left| \tilde{U}_T \right|^2 = |r_L|^2 \left[\left| \tilde{U}_F \right|^2 + \left| \tilde{U}_{M1} \right|^2 + 2 \left| \tilde{U}_F \tilde{U}_{M1} \right| \cos(\Delta\phi_{F1}) \right] \quad (2.2-9)$$

where $\Delta\phi_{F1}$ is the phase difference between the \tilde{U}_F and \tilde{U}_{M1} which is the main cause of the rotation of the irradiance pattern. Because the $\left| \tilde{U}_F \right|^2$ and $\left| \tilde{U}_{M1} \right|^2$ show no effect on rotation of the irradiance pattern, the only one term concerning to the phase is $2 \left| \tilde{U}_F \tilde{U}_{M1} \right| \cos(\Delta\phi_{F1})$. The phase of the \tilde{U}_{M1} rotates with the position of the scanning beam so that the cosine interference term causes a pattern rotation in the servo signal. Consequently, the rotation-free term is called the data signal, and the cosine interference term is called the servo signal. This analysis implies the design factor of the media that the optimum DPD signals are obtained with the high values of the land reflectance.

Case II : $r_L \neq 0, r_M = 0$, two tracks and two marks

The returning irradiance pattern is

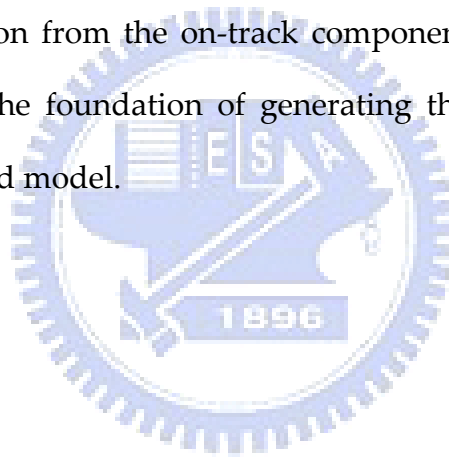
$$\begin{aligned} \tilde{I}_T \propto \left| \tilde{U}_T \right|^2 &= |r_L|^2 \left[\left| \tilde{U}_F \right|^2 + \left| \tilde{U}_{M1} \right|^2 + \left| \tilde{U}_{M2} \right|^2 \right. \\ &\quad + 2 \left| \tilde{U}_F \tilde{U}_{M1} \right| \cos(\Delta\phi_{F1}) \quad (a) \\ &\quad + 2 \left| \tilde{U}_F \tilde{U}_{M2} \right| \cos(\Delta\phi_{F2}) \quad (b) \\ &\quad \left. + 2 \left| \tilde{U}_{M1} \tilde{U}_{M2} \right| \cos(\Delta\phi_{12}) \right]. \quad (c) \end{aligned} \quad (2.2-10)$$

Term (a) in the (2.2-10) stands for the I_{SERVO} , as which is mentioned in case I, and term (b) stands for the type one crosstalk; finally, term (c) stands for the

type two crosstalk. Type one crosstalk is formed by the interference of the on-track mark and the adjacent track; likewise, the crosstalk in type two is generated by the interference between the on-track and off-track marks.

2.2.4 Summary

In this section, a different principle for analyzing the diffraction patterns and the origin of the signals has been reviewed. This method is found on the decomposition of the reflected light field due to the on-track and off-track marks on the detector. That the origin of the DPD servo signal is due to the phase of the diffraction from the on-track component has been shown. The Babinet principle is the foundation of generating the readout signal, servo signals of the proposed model.



2.3 Servomechanisms

To keep the laser beam in focus to a correct position is important for reliable data storage and retrieval. During read/write/erase operations, keeping the spot in focus and following the track in the radial direction are two major concerns. The demand for the position control stems from the mechanical deviations of the drives and disks both in focusing and tracking directions.

The spot size on the disk surface for a DVD-system has a diameter of less than a micrometer. To maintain this small spot size tightly focused, the position of the objective lens must be constantly adjusted to correct for the axial motion of the disk surface as the disk spins. The position of the objective lens is controlled by the servomechanisms consisting of two parts: focus servo and tracking servo, as depicted in Fig. 2.3-1. These servomechanisms are described below, followed by an explanation of the laser beam position control system used for seeking and track following.

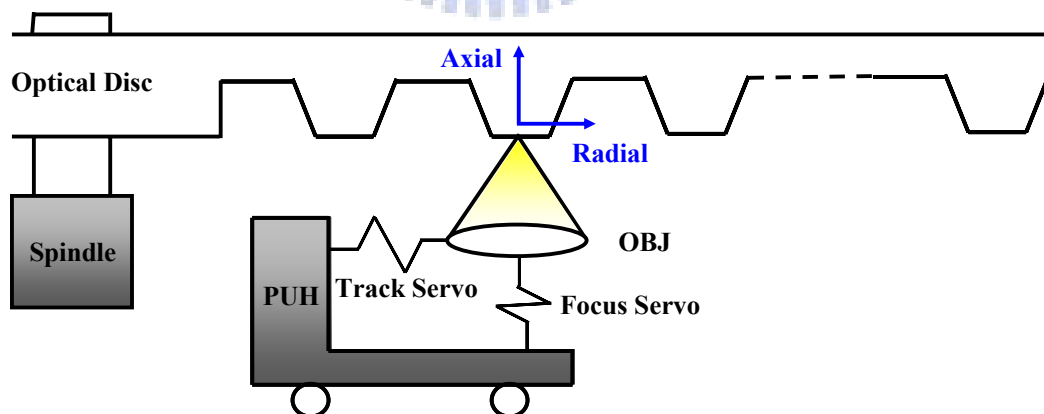


Fig. 2.3-1 Schematic diagram of pick-up head with focus servo and tracking servo

2.3.1 Focus Control

The optical data storage system needs the focus control system to generate the feedback signal used to correctly indicate the degree and the direction of focus error. There are three common methods used to achieve the focus control: The obscuration method, astigmatism method, and the differential spot-size method.

The astigmatism method uses the astigmatic lens to focus the reflected laser beam onto the quadrant detector to generate focus error signal, illustrated in Fig. 2.3-2. In perfect focus, the distribution of the reflected laser beam is equal on the four elements of the quadrant detector. Nevertheless, if the defocus arisen from the axial run out is introduced, two mutually perpendicular elliptical laser spot along the optical axis in sagittal and tangential directions will be formed.

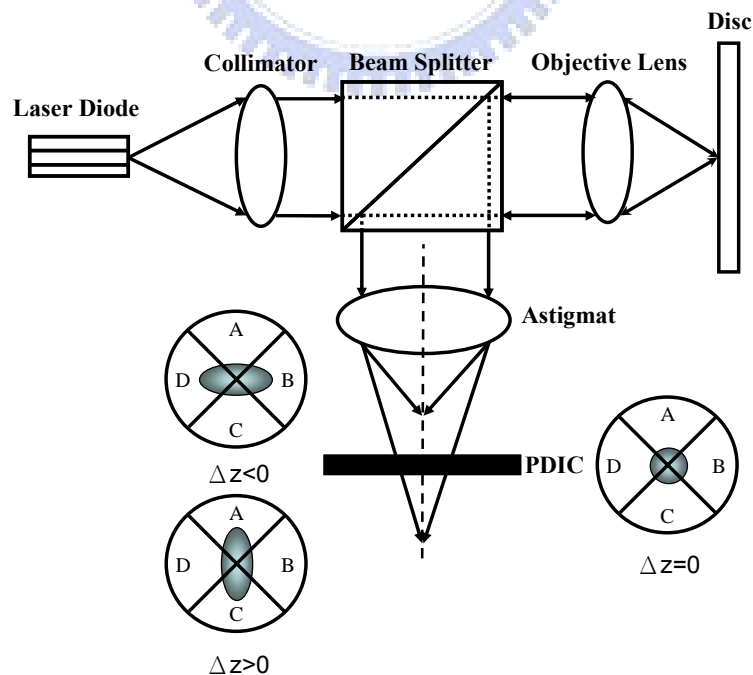


Fig. 2.3-2 Astigmatism focus error method

The unequal distributions of light on the quadrant detector generate a focus error signal (FES), as formulated in (2.3-1). This signal is normalized with respect to the light level to make it independent of laser power and disk reflectivity. This curve is often called the “S-curve” because of its shape.

$$FES = \frac{(A + C) - (B + D)}{A + B + C + D} \quad (2.3-1)$$

2.3.2 Tracking Control

The beam returning from the disk contains first-order diffraction patterns; their intensity depends on the position of the spot on the tracks, and varies with the spot moving away from the track center. The same quadrant detector that is used to generate the focus error signal can be used to generate the tracking error signal (TES), and the TES is the normalized difference of the current from the split detector, as formulated in (2.3-2).

$$TES = \frac{(A + B) - (C + D)}{A + B + C + D} \quad (2.3-2)$$

The TES peaks when the laser spot passes over the edge between the land and the groove and reset to zero when the spot is at the center of the track or land. The split detector can sense the relative position of the spot to the track center, and provides a feedback signal to the close-loop servo, as depicted in Fig. 2.3-3.

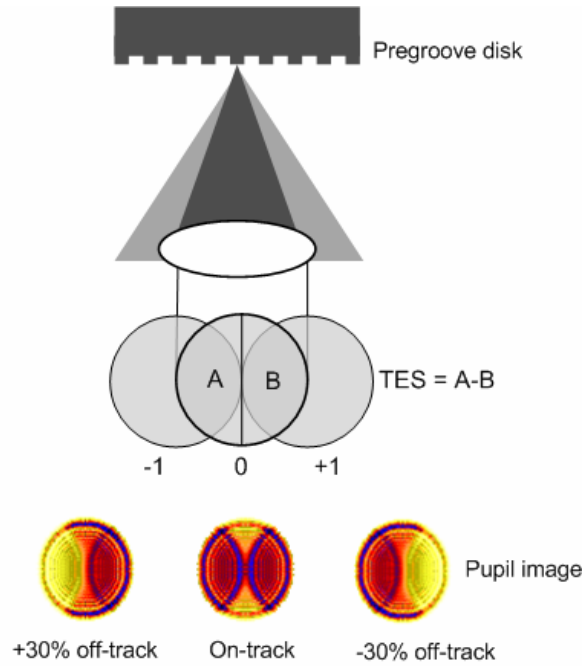


Fig. 2.3-3 The push-pull tracking method

The tracking mechanism is accomplished by a compound actuator, which consists of a coarse actuator and a fine actuator. The coarse actuator is usually a rail-mounted carriage driven by the linear voice coil motor. The fine actuator acts to produce a small radial displacement on the laser spot for a short track jump. The compound tracking actuator configuration has advantages over a single actuator not only in track following performance, but also when seeking between tracks.

In practice, mechanisms for extracting TES from the reflected beam depend on the disc format. Tracking error sensing is usually achieved with either: push-pull method, three-beam, differential push-pull, and differential phase detection. The relationships between the different disc formats and the tracking schemes are tabulated in Table 2.4. All schemes, when combined with appropriate closed-loop servos, can hold tracking errors to less than 0.01 mm to reduce crosstalk.

Table 2.4 The relationships between the different disc formats and the tracking schemes

Disc Formats	Tracking Methods
CD-ROM	Three-beam Method
DVD-ROM	Differential Phase Detection (DPD) Method
CD-R/RW	Push-pull (PP) Method
DVD±R/RW	or
DVD-RAM	Differential Push-pull (DPP) Method

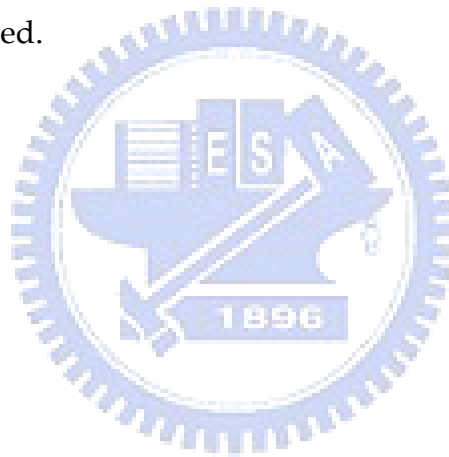
2.3.3 Servo Implementation Challenges ^[10]

Any defects of the wavefront imported by the imperfection factor of the optical components in the ODS system affect the performance of the servomechanism in various ways. An typical example is feedthrough due to the interference of the tracking error signal into the focus error signal.^[8] Feedthrough is any change in the focus error signal caused by the track crossing operation, and will lead to the laser spot out of focus. Minimizing or eliminating feedthrough is important during seeking where you need to maintain focus throughout the track crossing.

Feedthrough is a special case for a writable or re-writable disc, such as DVD±R and DVD±RW, which have pregrooved structure on it. Feedthrough becomes a serious problem at the beginning and at the end of the seek process. Because the scan velocity is low, the focus servo tends to respond to this kind of false focus-error signal. The feedthrough is affected by several factors. Firstly, it's the assembly issue including the misalignment of the detector or

the objective lens. Following up, the quality of the media is taken into consideration. The birefringence of the substrate will lead to a birefringence-induced astigmatism. Vertical birefringence of the substrate leads to a phase retardation of the returning beam.^[11] The third factor is the wavefront aberration including coma and astigmatic aberrations.

The origin and the influence on the servo signals of feedthrough will be discussed in the **Chapter 4**. The feedthrough is measured during the track crossing of one trackpitch in a DVD+R system as a demonstration. The effects imported by the coma and astigmatism aberrations on the feedthrough will be simulated and discussed.



2.6 Summary

In this chapter, the basics of the diffraction theories are reviewed. The connection and the comparison between the scalar and vector diffraction theory are formulated and organized. The Babinet principle which is used to decompose reflected light field and form data signal, servo signals, and crosstalks is the foundation of the signal process of this thesis. The optical model based on the simplified vector diffraction theory and the Babinet principle will be constructed in **Chapter 3** supplemented with the tolerance and jitter analysis.



Chapter 3

Simulation Model

In this chapter, the optical components used to construct the ODS system is discussed firstly, and the optical model is built based on the aforementioned principles in **Chapter 2**. The tolerance issue becomes more and more important as the growing of the storage density, and this factor will incorporate into the proposed optical model to observe the impact on the data signal and the servo signals. Jitter is an important evaluation factor of the signal in the ODS system; therefore, the basics of the jitter analysis from the optical point of view will be presented at the end of **Chapter 3**.

3.1 Simulation Description

In the design process of the ODS system, the physical structure of the optical disc, the data format and the design of pick-up head has been standardized for the compatibility of all kinds of discs, such as the wavelength of the laser diode, the numerical aperture of the objective lens. Different composing components are used for various focus servo and tracking servo adopted by different companies. In this thesis, the simulation framework is based on the optical pick-up head provided by ASUSTek computer Inc. The purposes of the optical pick-up head are to transmit the laser beam to the disc, to focus the laser beam to a diffraction-limit spot, and to transmit the information on the disc to the detector as the readout or the servo signals. In Fig. 3.1-1, the configuration of the DVD pick-up head system

is demonstrated.

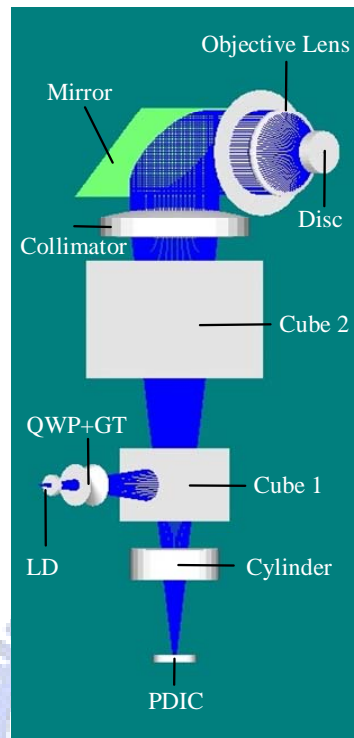


Fig. 3.1-1 The configuration of the simulated DVD system

The light of wavelength $\lambda = 660 \text{ nm}$, emitted from a laser diode is brought to the quarter wave plate (QWP) combined with a grating (GT) to generate a zero order and ± 1 orders light beams and to change the polarization state from linear to circular polarization. The beams are then collimated and focused on the disc by a collimator and an objective lens, accordingly. The recorded data on the disc will makes the distribution of the reflected light vary with the different reflectivities of the marks and land and this variation of the reflected distribution represents the digital data 0 or 1. Reflected from the disc, the light passes a cylindrical lens and is finally detected by the quad photo-detector. The readout signal can be generated as a result of the sum of

the quadrant signals.

Based on the pick-up head system from ASUSTek company Inc., the simulation model is determined. But in this thesis only main beam (zero order) is taken into consideration, the ± 1 orders light beams of the diffraction grating are omitted. Such way speeds up the simulation time. The components which just use to change the direction of the light or the split the optical paths of incident and reflected light can be omitted as well, such as folding mirror, cube 1, cube 2. Therefore, in this thesis only the laser diode, the collimator, the objective lens, the optical disc, the astigmatic lens, and the photo-detector are taken into account, as depicted in Fig. 3.1-2.

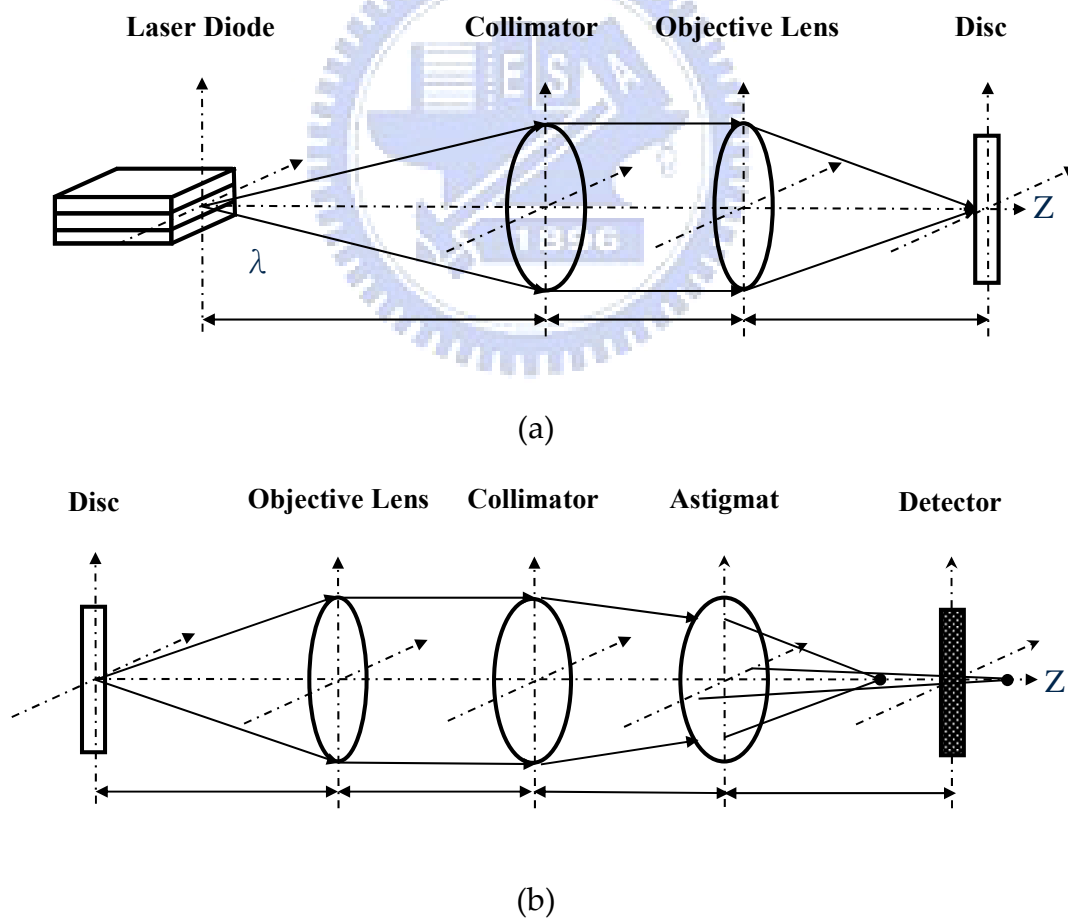


Fig. 3.1-2 The unfolded optical path of the simulation model: (a) The incident optical path, and (b) the reflected optical path

3.1.1 Readout Model

In the case of readout modeling, only one track is considered and the pre-groove structure is ignored to obtain the signal from the on-track marks. The readout signal created by the superposition of the sequential marks based on the Babinet principle is presented. The method of superposition of the sequential marks in the tangential direction (x-axis), sketched in Fig. 3.1-3, consists of two steps: in the first procedure, two isolated marks (with different lengths) are considered. The total field reflected from the recording layer is decomposed into components that consist of the isolated marks and the background reflection. In the subsequent procedure, the readout signal is then formed by superposition of a sequence of isolated marks of different lengths with varied spacing offset. The readout signal, called RF signal or eye-pattern, created by superposition of the sequential marks is formed by overlapping the signals of isolated marks more than 300 times to exhibit the eyepattern shown on the oscilloscope.

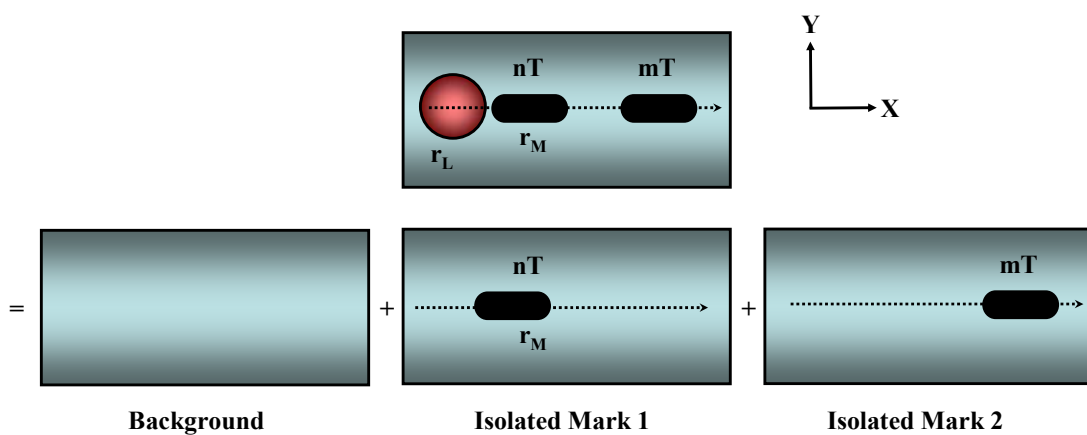


Fig. 3.1-3 Schematic diagram of the superposition of the sequential marks

3.1.2 Parameters

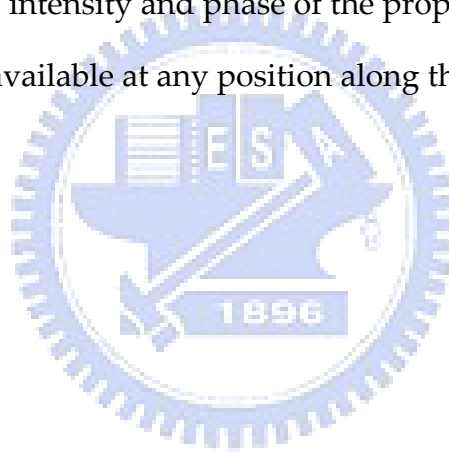
As mentioned in previous section, the simulation model is constructed by the laser diode, the collimator, the objective lens, the optical disc, the astigmatic lens, and the photo-detector and the main parameters of these optical components are listed in Table 3.1.

Table 3.1 Parameters of the DVD+R/RW System

LD Parameters	Value
Wavelength	660 nm
Astigmatism Distance	0.001 mm
Astigmatism Degree in X / Y direction	9.5 ° / 17°
Collimator Parameters	Value
Numerical Aperture	0.1116
Focal Length	17.8 mm
Objective Lens Parameters	Value
Numerical Aperture	0.65
Focal Length	3.05 mm
Astigmatic Lens Parameters	Value
Numerical Aperture	0.128
Focal Length 1	2.112 mm
Focal Length 2	2.217 mm
Photo-detector Parameters	Value
Length in X & Y Directions	0.058 mm
Division Line	0.004 mm
Disc Parameters	Value
Type	DVD+R/RW
Groove	Trapezoidal pre-groove
Refractive Index of the Substrate	1.58
Reflection Coefficient – Crystalline / Amorphous	0.55 / 0.38
Servomechanism	Type
Focus Servo	Astigmatism Method
Tracking Servo	Push-pull Method

3.1.3 Simulation Tool

Numerical calculations for this study was accomplished by use of DIFFRACT™, a FORTRAN-based diffraction modeling program that was created as a general purpose tool for optical data storage research. The user has a various functions of which different lenses, polarization optics, media, and detectors can be selected. DIFFRACT™ permits the user to choose different light beam distribution as the initial beam, and then it manipulates the propagation of this beam through the optical system by a plane-wave decomposition approach and Fourier techniques as mentioned in **Chapter 2**. The polarization state, intensity and phase of the propagating beam, as well as detector outputs, are available at any position along the optical path.



3.2 System Construction

In this section, three key optical component in the simulation model are verified by comparison the simulated results and the specifications offered by the each original company.

- Laser Diode

The verification begins with the discussion of the laser diode, since many optical components are chosen to match the properties of the laser diode. The light is emitted from the facet which has unequal width and length. As a result of this aspect ration, the divergence angles are different in the direction parallel and perpendicular to the laser junction. The spatial profile of the laser beam is therefore elliptical. A additional characteristic of the output laser beam is the astigmatism which leads to the different focal point of the beam parallel to the junction and that perpendicular to the junction.

The method used to verified the laser diode property is that the to make sure the divergence angle of laser diode simulated by the software is the same as that of the specification. Firstly, the intensity distribution is retrieved from the software. Secondly, the transformation of the intensity distribution from the distance to the angle is made to compare the divergence angle between the simulated results and the specification, which is sketched in Fig. 3.2-1.

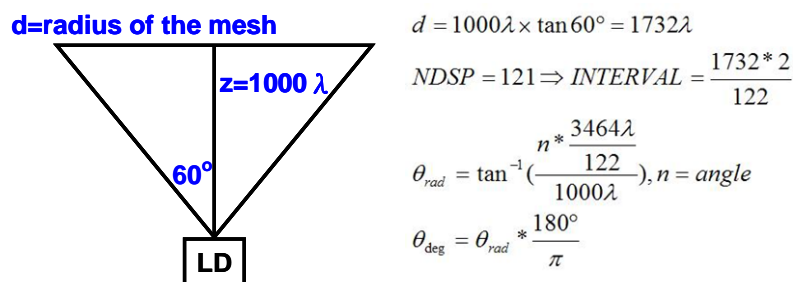


Fig. 3.2-1 Transformation from distance to angle

The comparison is shown in Fig.3.2-2.

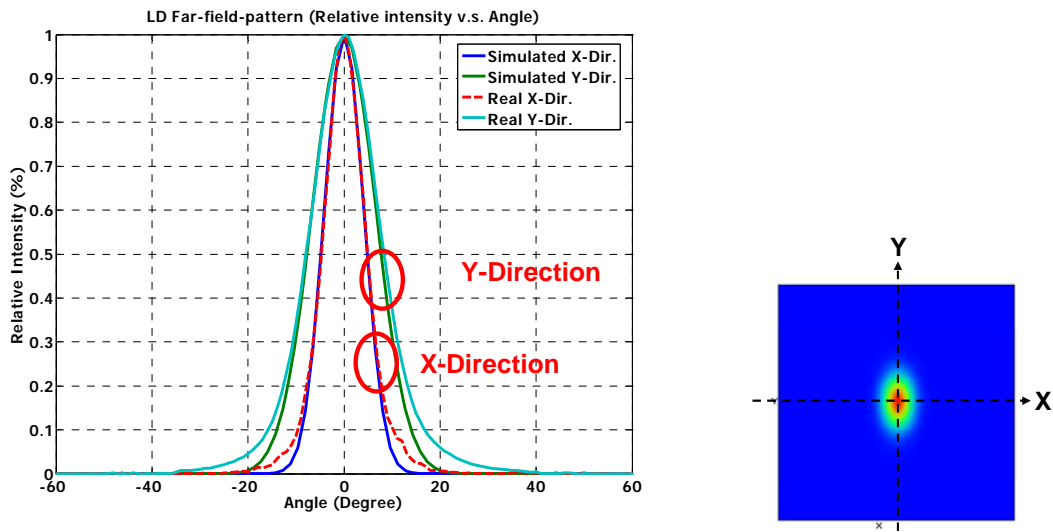
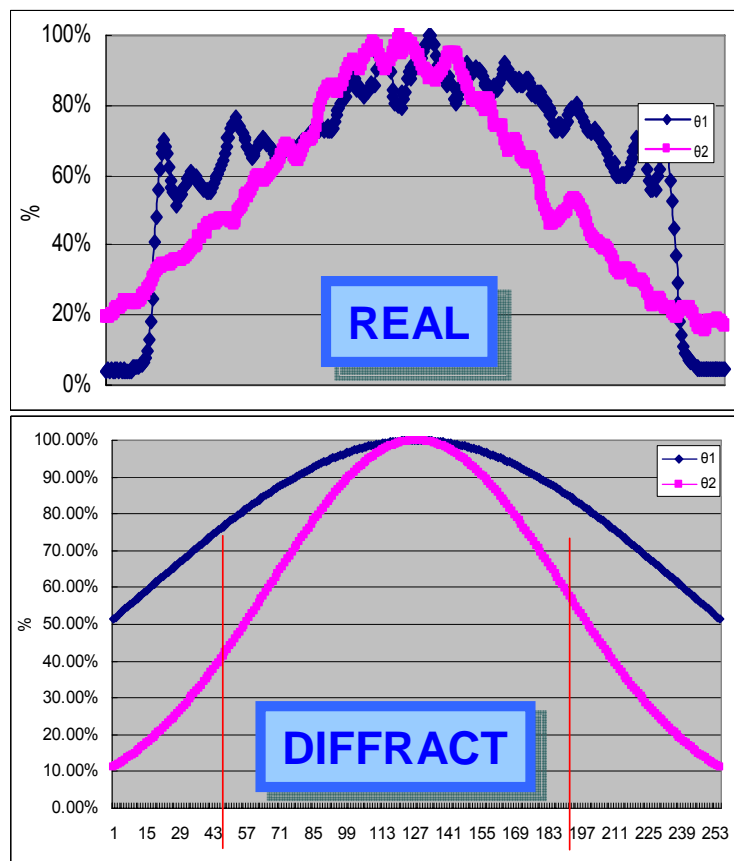


Fig. 3.2-2 The comparison of simulated results and the specifications of the laser diode

The comparison shows that the simulation is authentic and the divergence angle of the simulated versus the intensity distribution is matched together between the simulation and the specification.

- Collimator

The collimator will determine the amount of overfill of the lens (i.e. the amount by which the diameter of the incident light beam exceeds the aperture of the collimator) and this will affect the size of the focused spot on the disc. The method used to check the validity of the simulation is the comparison of the rim intensities. Fig. 3.2-3 shows two rim intensity plots of the simulation model and the real case. The comparison is made at the rim of the collimator (aperture diameter = 4 mm). The error in x and y direction is below 10% which is acceptable for further simulation.



(Aperture = 4 mm)	Real (a.u.)	Simulated (a.u.)	Error (%)
X Direction	35	32	8.57
Y Direction	65	71	9.23

Fig. 3.2-3 The comparisons of the rim intensities between the simulation and the real case

- Objective Lens

The objective lens is the key component used to achieve the diffraction-limit spot size on the disc. The most important feature of the objective lens is the spot size and the checkpoint here is the ratio of the spot size between the simulation and the real case. The simulated FWHM spot size in the x- and y-direction is shown in Fig. 3.2-4. In this study, the author uses DIFFRACT™ as the simulation tool to simulate the lens

property in the ODS system. Fig. 3.2-4 is the caption of the output signal generated by DIFFRACT™.

```

PEAK INTENSITY AND FWHM
*****

Z-component of polarization is unavailable but may be computed if necessary
*****

Include Z-component of polarization (Y/N)? N

Please stand by...

-----
Peak Intensity= .627E+00  XPEAK=          .00  YPEAK=          .00
-----

Save Peak Intensity, XPEAK, YPEAK in SIGNAL array by entering their
respective ID numbers in the range [0-99] (ID1, ID2, ID3):  10 11 12

Compute FWHM of the beam or return to menu (C/R)? C
Direction along which FWHM is measured (Theta:0-180):      45.000000

-----
Theta= 45.00    FWHM=    .86
-----

To save FWHM in SIGNAL array enter its ID in the range [0-99]: 15

Press RETURN to continue...

Compute FWHM of the beam or return to menu (C/R)? C
Direction along which FWHM is measured (Theta:0-180):      135.000000

-----
Theta=135.00    FWHM=    .78
-----

```

Directions	X	Y	Ratio (X/Y)
Real (a.u.)	0.505	0.460	1.097
Simulated (a.u.)	0.860	0.780	1.102

Fig. 3.2-4 The focused spot size of the simulation and the real case

The intensity ratio of x-direction to the y-direction between the simulation and the real case is almost the same and the difference can be regarded as the numeric error.

3.3 Tolerance Issues

As the increasing storage density of the ODS system, the depth of focus which is inversely proportional to the square of the NA becomes smaller. The depth of focus defines the accuracy with which the objective lens position must be maintained with respect to the disc surface. The smaller the depth of focus, the less tolerance the system has for the media tilt, the more difficult job for the focus servo. The tilt and defocus are two common error in the ODS system, and the influence of these two errors will be introduced in the following sections.

3.3.1 Tilt Effects

The disc tilt will produce aberrations that consist primarily of coma with a slight amount of astigmatism.^[12] The focused spot shows the expected spreading of the light resulted from coma aberration in the direction of tilt, as illustrated in Fig. 3.3-1. The primary coma aberration caused by disc tilt is considered and calculated from equation shown in (3.3-1):

$$\frac{W_{\beta}}{\lambda} = -\frac{1}{2} NA^3 \beta \frac{d}{n^* \lambda} \left(1 - \frac{1}{n^2} \right) \quad (3.3-1)$$

where β is the tilt angle with respect to radial direction, and d is the substrate thickness, and n is the refractive index of the substrate.

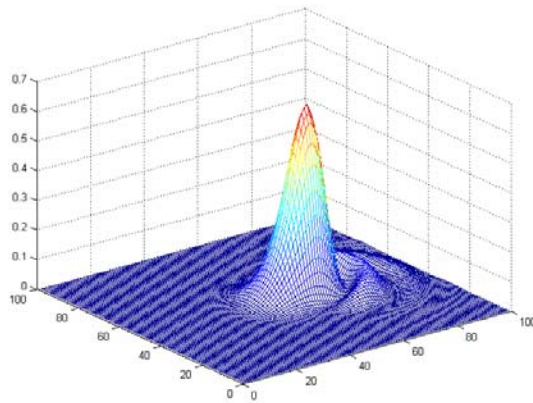


Fig. 3.3-1 The focused spot with coma aberration of -1λ

The coma aberration W_β is about -1λ with $\beta = 1.5^\circ$, $d = 0.6$ mm, and $n = 1.58$, respectively. The disc tilt distorts the shape of the focused spot and the aberrated spot may cover the neighboring tracks which lead to a crosstalk and produce an offset of the focused spot from the center of the track. The amplitudes of the readout and the servo signal drop in magnitude as the tilt becomes larger. These drops in magnitude is owing to the vignetting (i.e., deviation of the beam from its nominal return path) and the broaden spot size.

From the DVD specification, the tolerance of the radial tilt and the tangential tilt should be less than $\pm 0.8^\circ$ and $\pm 0.3^\circ$, respectively. The deviation of the tilt angle is more and more serious with the radius. In the next generation systems which use shorter wavelengths, tracking servo becomes more sensitive to disk tilt because of the increased thickness of the substrate and the increased N.A. of the objective lens.^[13] The spot on the disc with coma aberration is not perfect circularly symmetric any more.

3.3.2 Defocus Effects ^[14]

When an optical disc is read, the most important aberrations induced by the defocus effect are defocus (W_{20}) and spherical aberration (W_{40}). The defocus aberration and the spherical aberration are considered and calculated from the equations shown below:

$$\frac{W_{20}}{\lambda} = \frac{n-1}{2n} \frac{NA^2}{\lambda} \Delta d \quad (3.3-2)$$

$$\frac{W_{40}}{\lambda} = \frac{n^2-1}{8n^3} \frac{NA^4}{\lambda} \Delta d \quad (3.3-3)$$

where Δd is the defocus distance from the ideal focus position, NA is the numerical aperture of the objective lens, and n is the refractive index of the substrate. The aberrated spots on the focal plane are shown in Fig. 3.3-2.

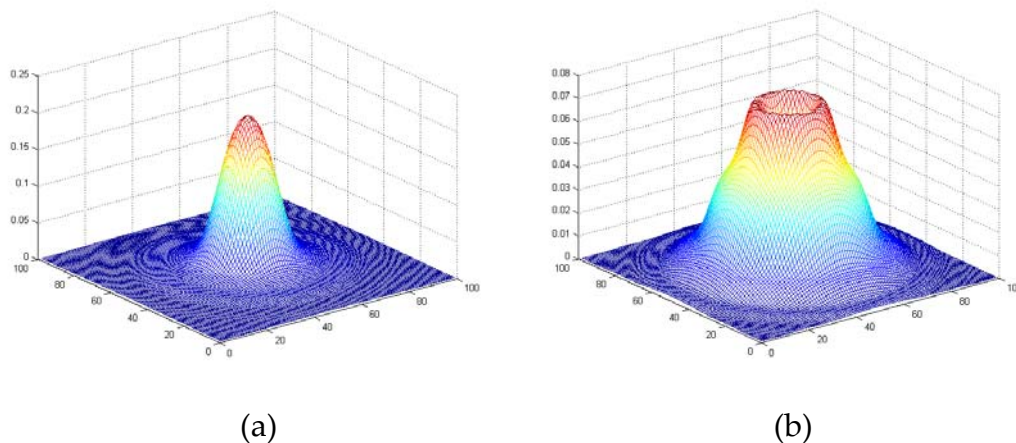


Fig. 3.3-2 The focused spot with (a) spherical aberration, and (b) defocus aberration of -1λ

The thickness variation of the transparent substrate of the optical disc is the key characteristic for an optical disc and has a great influence on the readout and servo signal. The spherical aberration can be corrected by the

objective lens which is designed in such a way that the spherical aberration has been compensated. The defocus aberration results in the change in the depth of focus which leads to a tighter tolerance in focus servo.

In an optical drive, the zero crossing point of the FES is not coincident with the minimum jitter point, as illustrated in Fig. 3.3-3.

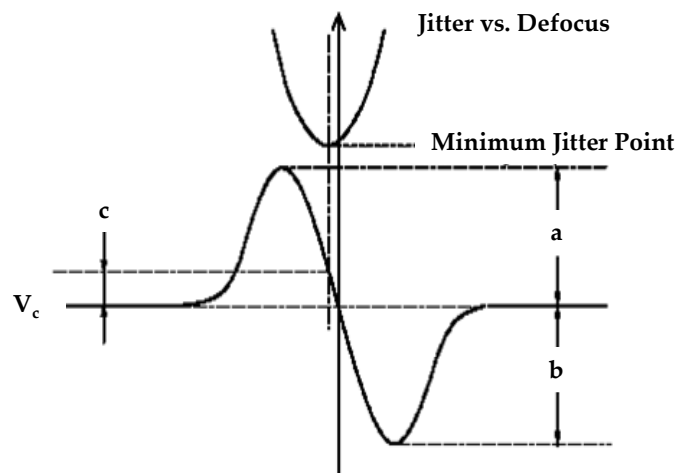


Fig. 3.3-3 The relationship between the FES and the plot of Jitter vs. Defocus

The defocus distance is defined as the ratio of deviation of the FES level at the minimum jitter point from the reference voltage (V_c), as formulated in (3.3-4).

$$Defocus = \frac{c}{a+b} \times 100\% \quad (3.3-4)$$

3.4 Jitter Analysis

Jitter is the standard deviation of the time variations of the binary read signal. The binary read signal is created by a slicer, after feeding the RF signal from the RF signal channel through an equalizer and the low-pass filter. The jitter of the leading and trailing edges is measured relative to the phase-lock loop (PLL) clock and normalized by the channel bit clock period. In other words, the jitter expresses how much the structures (marks) recorded to a disc deviate from the length they are supposed to have. Jitter should be as low as possible to provide a reliable readout signal, but there are many causes will lead to jitter such as the noise of the optical components, the inter-symbol interference, and the variation of the embossed or burn marks, etc.

There are two kinds of definitions of jitter:

1. Time Interval Analysis (TIA)^[16]: The TIA test will create a histogram of the length variations of each mark length. Due to the imperfection, marks will never have the exact length they are supposed to have (3T, 4T, 5T... 10T, 11T and 14T), but will differ more or less. A perfect test result shows spaces between each peak which means that marks supposed to have a length variation x which is always in $-0.5 \sim +0.5$ so that we can distinguish each peak easily. The standard deviation of the results of this test is the Jitter, which is shown in Fig. 3.4-1. This is the general method adopted by the optical disc drive.

2. Window occupation: The detection window is defined as the width of 1T (1T=0.133 μ m), and the jitter is defined as the width of the signal at the crossing-point of the RF signal. The window occupation is the ratio of the

jitter to the length of the detection window.

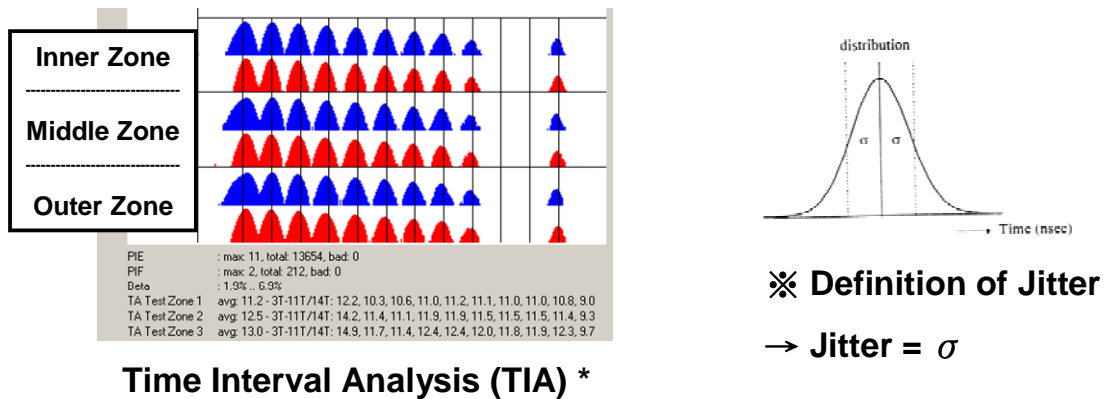


Fig. 3.4-1 Time interval analysis and the definition of jitter

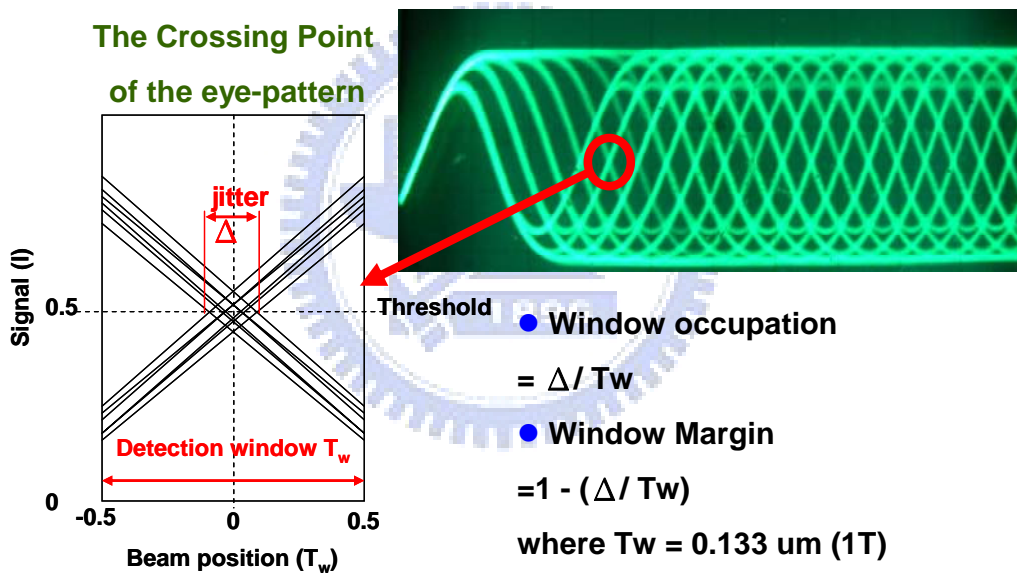


Fig. 3.4-2 Window occupation method

These two kinds of methods provide a possible way to observe the jitter which is an important evaluation factor of the readout signal in the ODS system. In this thesis, the widow occupation method is used to calculate the jitter of the simulated ODS system. The widow occupation method is easier to obtain than the TIA method does but still can give a correct trend of the quality variation of the readout signal.

3.5 Summary

In **Chapter 3**, the simulation condition is revealed in the first section, and the readout model based on the Babinet principle is introduced. The readout signal can be generated by the method of superposition of the sequential marks will demonstrated in **Chapter 4**. The tolerance analysis and the jitter analysis presented in **Chapter 3** will be used to analyze the ODS system with tilt and defocus.

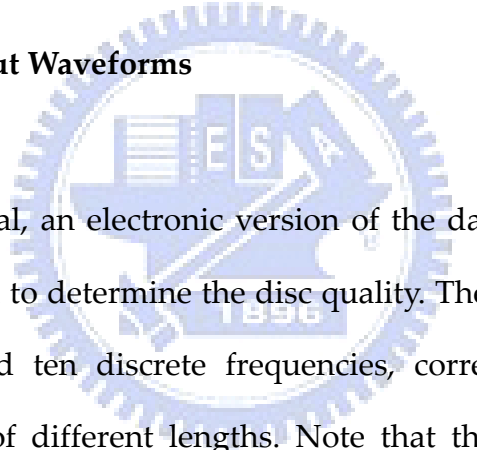


Chapter 4

Simulation Results

In **Chapter 3**, the optical model based on the aforementioned principles is built and the tolerance and jitter analysis are introduced for emphasizing the influence of the tolerance and the aberrations on the readout signals. The results of **Chapter 4** are obtained by the Babinet principle and the jitter analysis mentioned in the **Chapter 3**.

4.1 Results 1 – Readout Waveforms



The readout signal, an electronic version of the data information on the disc, can be processed to determine the disc quality. The signal reflected from the disc is comprised ten discrete frequencies, corresponding to the ten discrete pit or land of different lengths. Note that the various frequencies modulate the intensity of the reflected light with the different pit or land lengths. The highest-frequency component, called 3T, is generated by the shortest pit or land length and the lowest-frequency one, called 14T, is produced by the longest pit or land length. The signal reflected from the disc, produced by encoding procedure, is often called the RF (radio frequency) signal. The varying periods of the sine waves correspond to the periods of time required to read the various pit lengths.

The RF signal is generated by the superposition of the sequential marks based on the Babinet principle. There are two steps in this method: in the first

step, the isolated signals from different lengths of the pits on the disc are extracted from the signal file generated by the simulation tool. The reflected intensities of the isolated marks are shown in Fig. 4.1-1. The signals of the photo-detector are modulated by the lengths of the pits from 3T to 14T (without 12T and 13T) which can be observed in Fig. 4.1-1 from the left to the right.

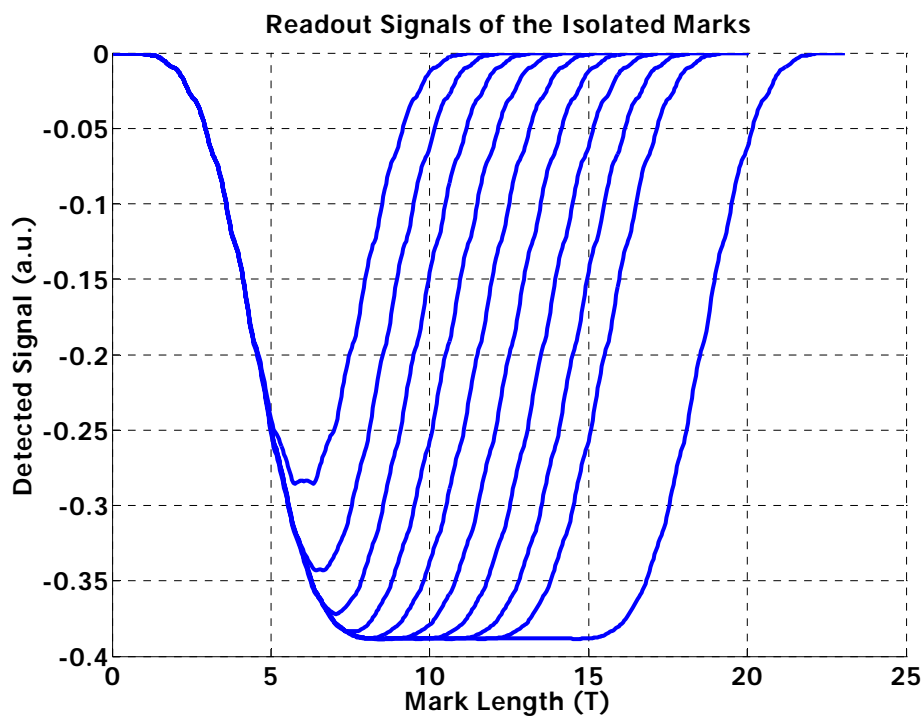


Fig. 4.1-1 The readout signals of the isolated marks from 3T to 14T (without 12T & 13T)

In the second step, the isolated signals of the pit lengths from 3T to 14T (without 12T & 13T) is manipulated by Matlab® with the method of random overlapping the isolated signals to exhibit the eyepattern observed on the oscilloscope. The readout signal, called RF signal or eye-pattern, is formed by superposition of a sequence of isolated marks of different pit lengths with

varied land spacing offsets and overlapping the signals of the isolated marks more than 300 times to obtain the a close result compared to the experimental result. As revealed in Fig. 4.1-2 and Fig. 4.1-3, the trigger level is different, and therefore the direction is opposite. Nevertheless, the eyepatterns in two figures are very clear and similar. As you can observed in Fig. 4.1-1 and Fig. 4.1-2, there is an error (depression) near the peak value of the mark length $3T$. This nonlinear phenomenon arises due to the inter-symbol-interference in the readout waveform because the size of the laser spot approaches to that of the length of $3T$.^[15]

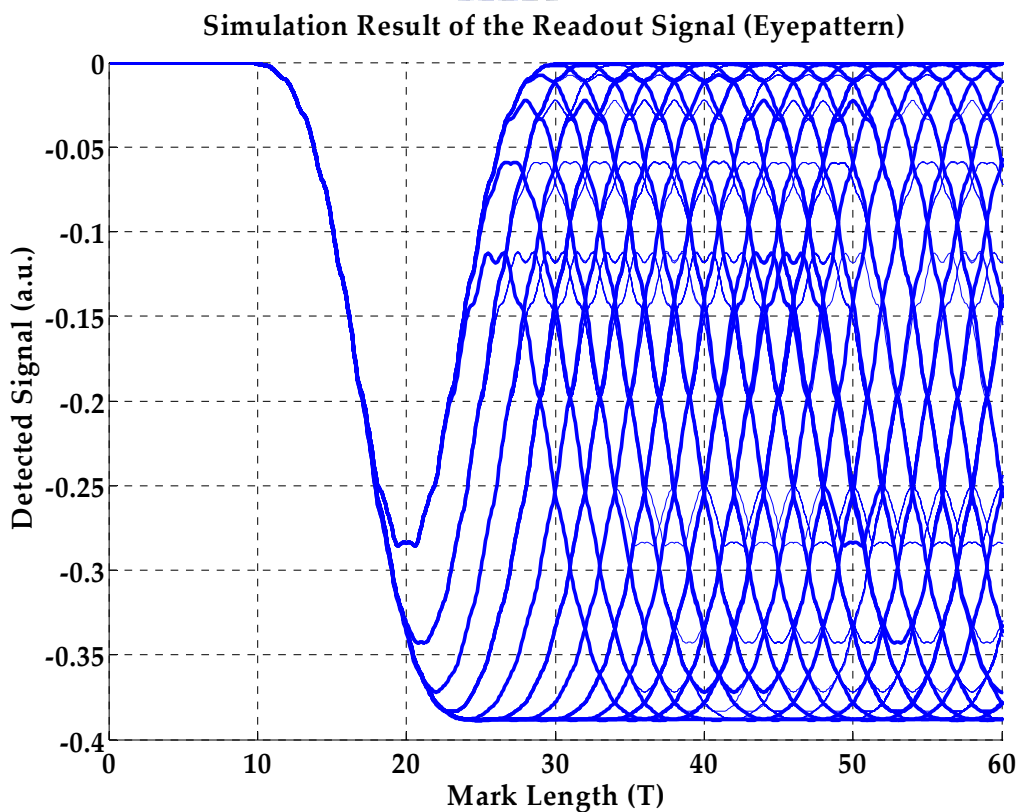


Fig. 4.1-2 The simulation result of the readout signal (eyepattern)

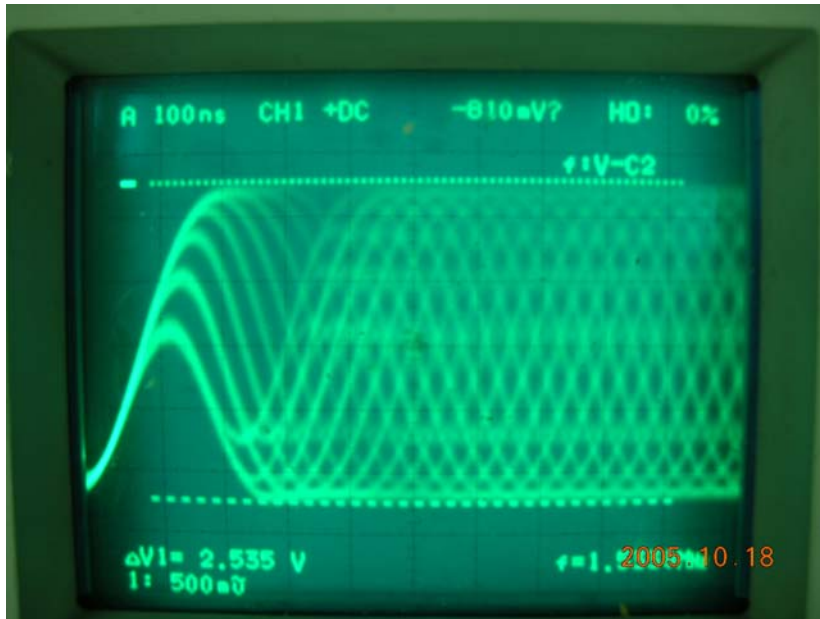


Fig. 4.1-3 The experimental result of the readout signal (eyepattern)

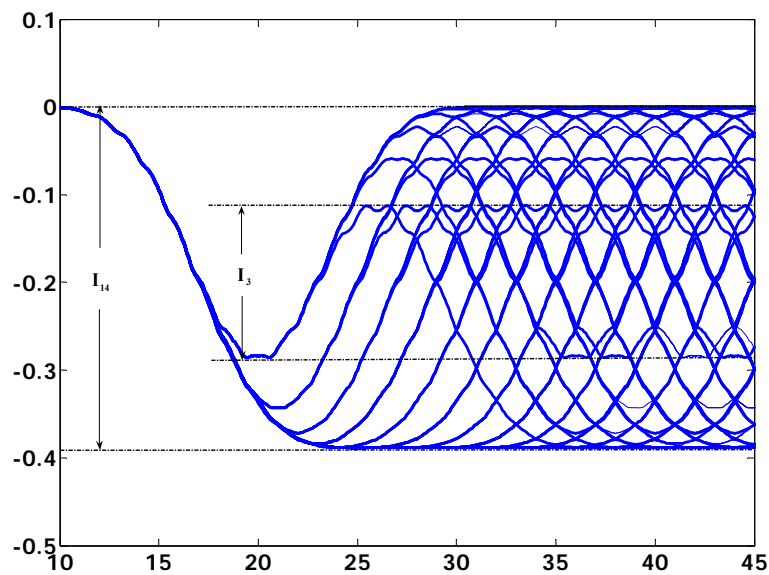


Fig. 4.1-4 Readout signals from spaces and marks

From the DVD+R specification, the readout signal, also known as RF signal, is obtained by summing the currents of the four elements of photo

detector, as illustrated in Fig. 4.1-4. These currents are modulated by the information recorded as the marks and lands on the information layer of the disc. The amplitudes of these modulated signals should follow the requirements listed in (4.1-1) and (4.1-2).^[16]

$$\frac{I_3}{I_{14}} \geq 15\% \quad (4.1-1)$$

$$-5\% \leq \left[\frac{\frac{I_{14}}{2} - \frac{I_3}{2}}{I_{14}} \right] \leq 15\% \quad (4.1-2)^*$$

where the amplitude I_{14} is the peak-to-peak value of the RF signal generated by the longest mark (14T). The amplitude I_3 is the peak-to-peak value generated by the shortest mark (3T). (4.1-2) is called the signal asymmetry (Beta) which shows how well pits and lands on a disc are balanced. These two requirements are used to give a qualification analysis of the reliability of the simulated readout signal.

Table 4.1 The comparison of the requirements between experiment and simulation results

	$\frac{I_3}{I_{14}}$ (%)	$\frac{\frac{I_{14}}{2} - \frac{I_3}{2}}{I_{14}}$ (%)
RF signal (Experiment)	39.20	8.50
RF signal (Simulation)	73.58	13.21

From the comparisons, two conclusions can be drawn as listed bellowed:

1. The simulated RF signal has a better amplitude ratio (73.58%) than the experimental result (39.20%). Because the simulation model is ideal, which are no aberrations or tolerance issue are considered, the simulation results shown the higher signal contrast ratio make sense.
2. The RF signal of the experiment has a better beta value (8.50%) than the simulation result (13.21%). The overlapping sequence can not simulate the situation of the real case in an accurate way, and therefore the balance between the pits and lands of the simulation result is poorly compared with the experimental result.



* This is the modified signal asymmetry condition, the original formula from the specification is as followed:

$$5\% \leq \left[\frac{\frac{I_{14H} + I_{14L}}{2} - \frac{I_{3H} + I_{3L}}{2}}{I_{14}} \right] \leq 15\%$$

But the I_{14L} and I_{3L} are coincided with the zero level which is measured when no disc is inserted and the I_{14H} and I_{3H} are the same as I_{14} and I_3 .

4.2 Results 2 – Servo Signals : FES & TES

The servo signal is a very important factor for maintaining the spot on the desired track of the information layer. The laser spot is feedback control by the focus and tracking methods mentioned in the **Chapter 2**. The astigmatism method and push-pull method are adopted in the proposed model for the focus servo and tracking servo, respectively. The reliabilities of these two signals are inspected in the following.

- Focus Error Signal (FES)

The FES is produced by the astigmatism method under the condition of DVD+R disc without pre-groove structure on it. The corresponding intensity distributions of the laser spot on the photo-detector at the three positions: (a) M (too-near), (b) P (in-focus), and (c) N (too-far) are shown in Fig. 4.2-1. The image position is changed with the disc position in the axial direction and the intensity pattern on the photo-detector is varied with the near (far) disc position to form the transverse (perpendicular) ellipse. According to this change in shape of the intensity pattern on the photo-detector, the FES, called S-curve, is created to feedback control the spot position in axial direction.

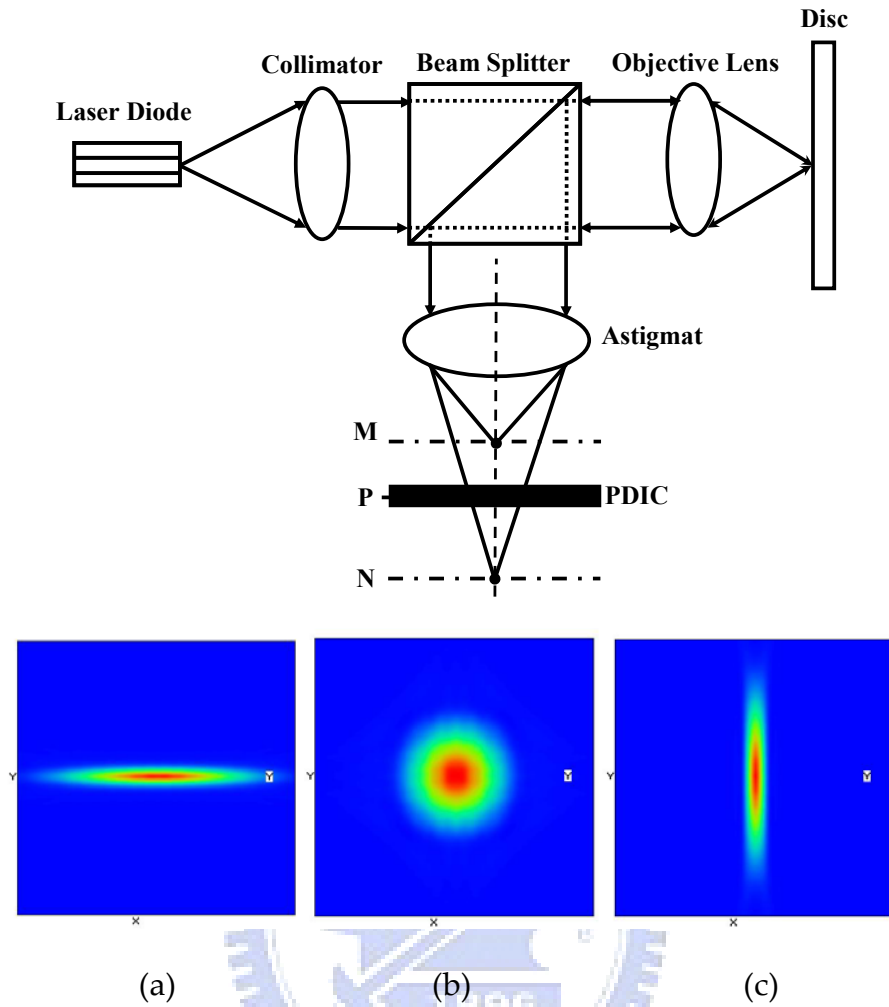


Fig. 4.2-1 The astigmatism method and the intensity distributions at position (a) M (too-near), (b) P (in-focus), and (c) N (too-far)

The S-curve is obtained by moving the position of optical disc in opposite directions, and the result is compared with the experiment to confirm the correctness of the generated FES. The comparison of the simulated S-curve and the experimental result is shown in Fig. 4.2-2.

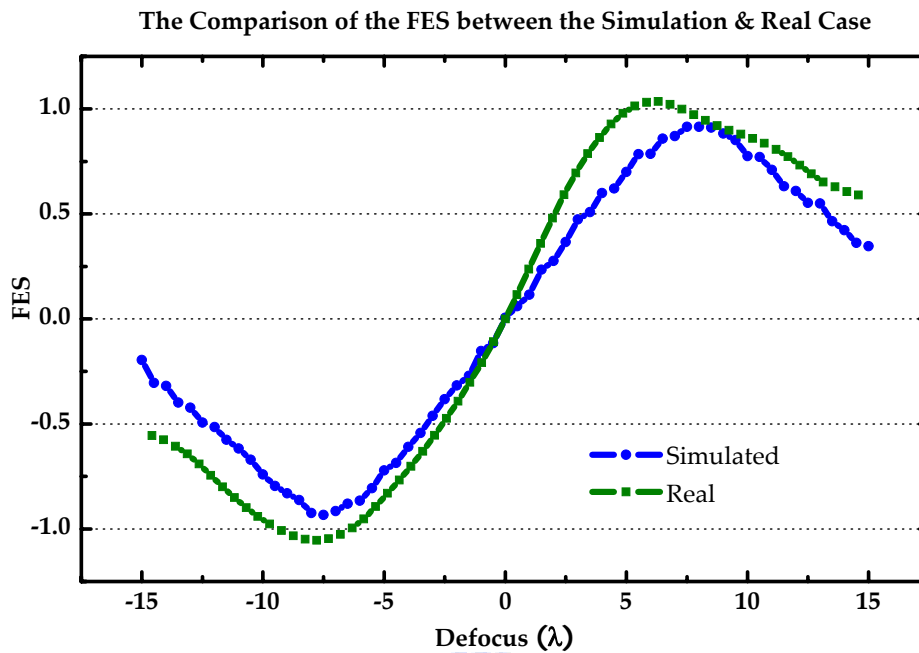


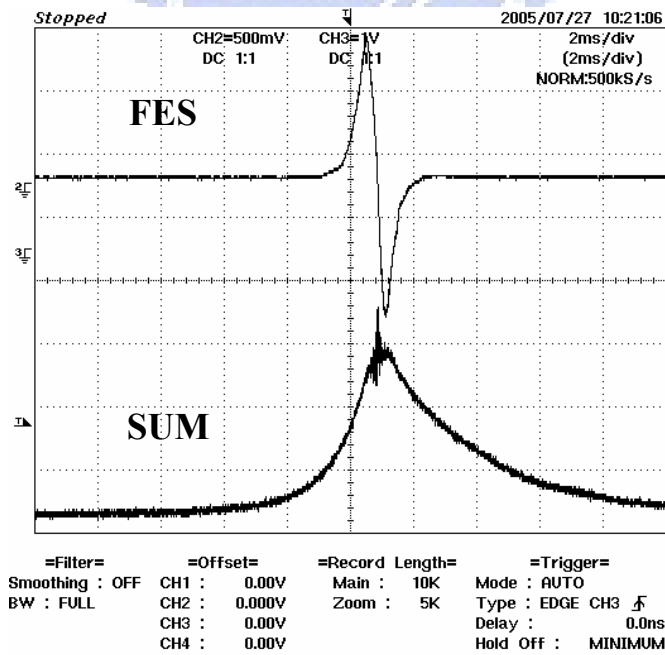
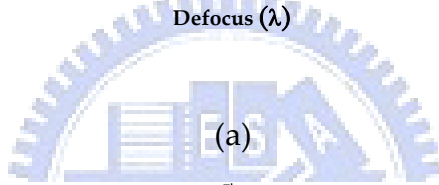
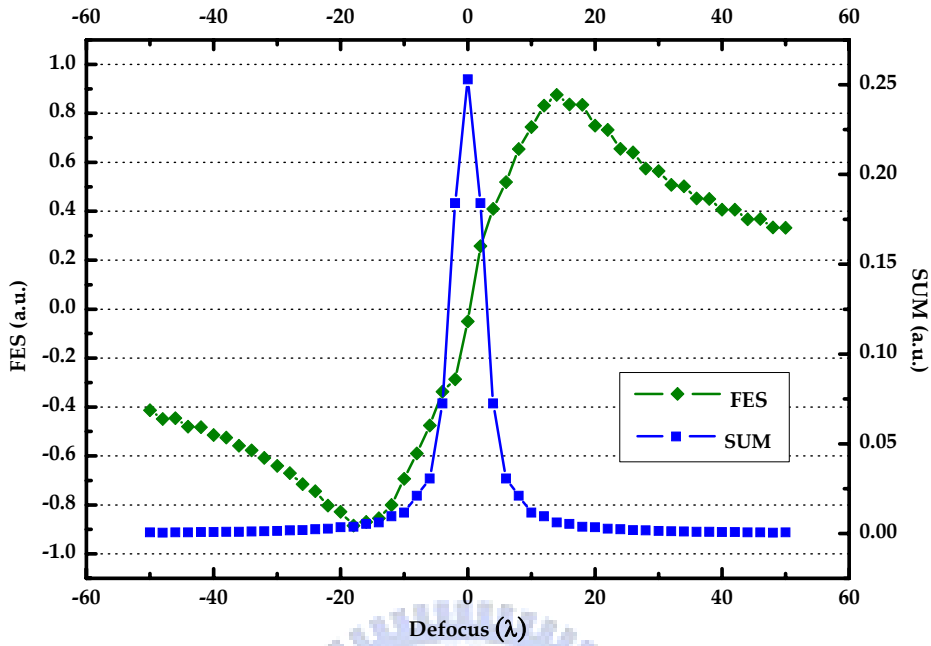
Fig. 4.2-2 The comparison of the FES between the simulation result and the experimental result

Whenever the optical drive is on, the first movement of the optical drive is to move the pick-up head to focus the laser spot on the information layer of the disc according to the FES provided by the focus servo. The linear range of the S-curve is the key factor for the focus servo, and the larger linear range makes the laser spot easier to achieve in focus. The linear range of the experimental result and the simulation result are listed in Table 4.2, which show the linear range of the simulation model (14.5λ) can satisfy the condition of the experiment (15λ).

Table 4.2 The comparison of linear ranges

	Linear Range (λ)
Simulated S-curve	14.5
Experimental S-curve	15.0

When the laser spot is in focus, the total reflected light from the information layer is maximum and the FES is approach to zero simultaneously. The total reflected intensity drops rapidly with the defocus distance from the focal plane. The relationship between the FES and the sum of the photo-detector is shown in Fig. 4.2-2. The sum signal of the photo-detector drops almost to zero within the boundaries of the linear range of the FES. In Fig. 4.2-3(b), it shows a experimental results which gives a close agreement with the simulation. Note that the oscillation near the peak of the sum signal is caused by the recorded marks on the disc.



(b)

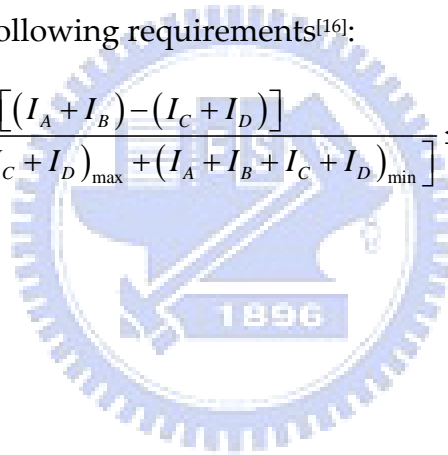
Fig. 4.2-3 The relationship between the FES and the sum signal on the photo-detector: (a) the simulation result, and (b) the signals from oscillator

- Tracking Error Signal (TES)

The tracking method in the proposed model is the push-pull method, which generate the TES by the difference signal between the two halves in the Read channel two when the focus of the laser spot scans cross the tracks. The TES peaks when the laser spot passes over the edge between the land and the groove and reset to zero when the spot is at the center of the track or land. The split detector can sense the relative position of the spot to the track center, and provides a feedback signal to the close-loop servo.

From the DVD+R specification, the peak-to-peak value of the push-pull signal shall meet the following requirements^[16]:

$$30\% \leq \frac{[(I_A + I_B) - (I_C + I_D)]}{[(I_A + I_B + I_C + I_D)_{\max} + (I_A + I_B + I_C + I_D)_{\min}]} \leq 60\%$$



4.3 Results 3 – Tolerance Analysis

The tolerance issue is the most important factor for the stability and the reliability of the optical drives. Tilt and defocus are two main tolerances should be paid a close attention. In this section, these two key elements are analyzed and discussed.

4.3.1 Tilt

The tilt of the objective lens or the disc will result in the distribution variation of the laser spot on the information surface with different tilt angle. (3.3-1) is adopted to simulate the coma aberration introduced by the tilt effect and such aberration is added onto the objective lens. The coma aberration $W\beta$ is about -1λ with $\beta = 1.5^\circ$, $d = 0.6$ mm, and $n = 1.58$, respectively. The simulation result of the RF signal with radial tilt of 1.5° is shown in Fig. 4.3-1.

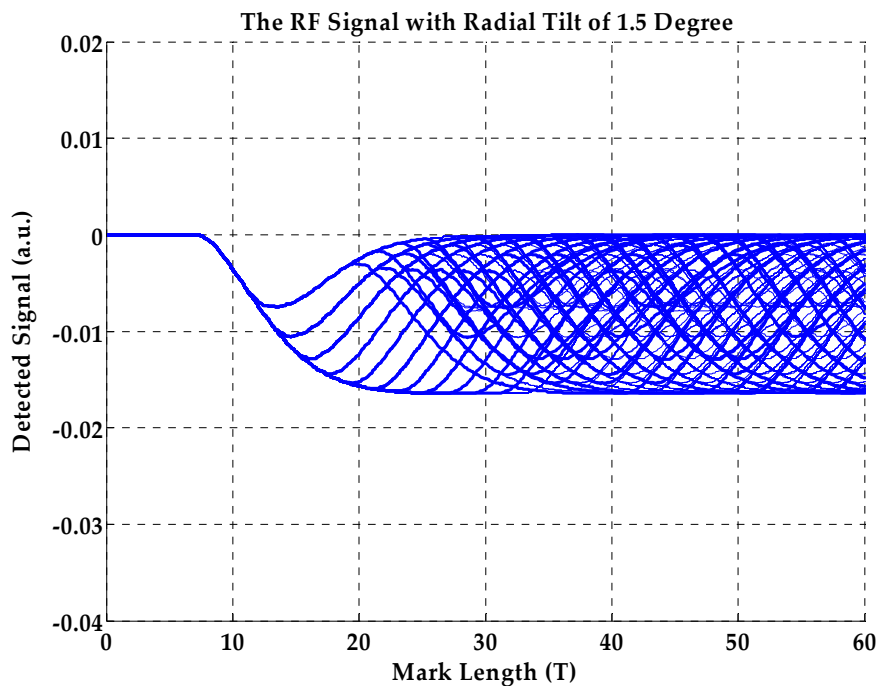


Fig. 4.3-1 The RF signal with radial tilt of 1.5°

Compared with the result shown in Fig. 4.1-2, the amplitude of RF signal decrease about a half of the ideal case and the eye-patterns in the RF signal become blurred. The jitter and amplitude of the eye-pattern with radial tilt of 1.5° is increased and decreased by a factor of 3.55x and 0.45x, respectively. The experimental results of the RF signals with different tilt angles are illustrated in Fig. 4.3-2. As the tilt angle increases, the amplitude of the RF signal reduces and the eyepatterns becomes vaguer from 0° to $30'$. The results are in close agreement with the calculated results.

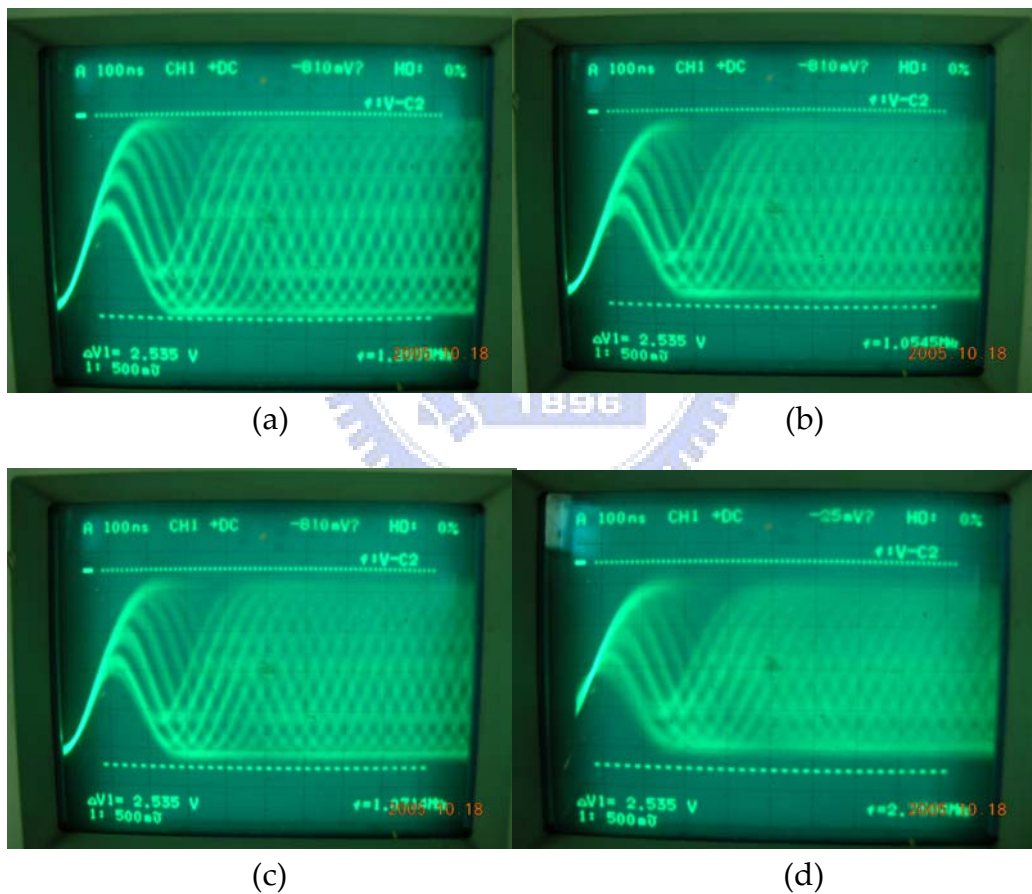


Fig. 4.3-2 The tilt effect upon the RF signal with different tilt angles: (a) 0° , (b) $10'$, (c) $20'$, (d) $30'$

The jitter value expresses how good the signal is and provides an easy way to evaluate the quality of the disc. The window occupation method is used for calculating the jitter in our simulation model. The jitter value is obtained by measuring the lateral deviation of mark length of 3T. The lateral deviation is defined as the distance between the positions of the zero crossing point of the simulated signal and the ideal signal of 3T. The variations in the amplitude and the jitter are shown in Fig. 4.3-3.

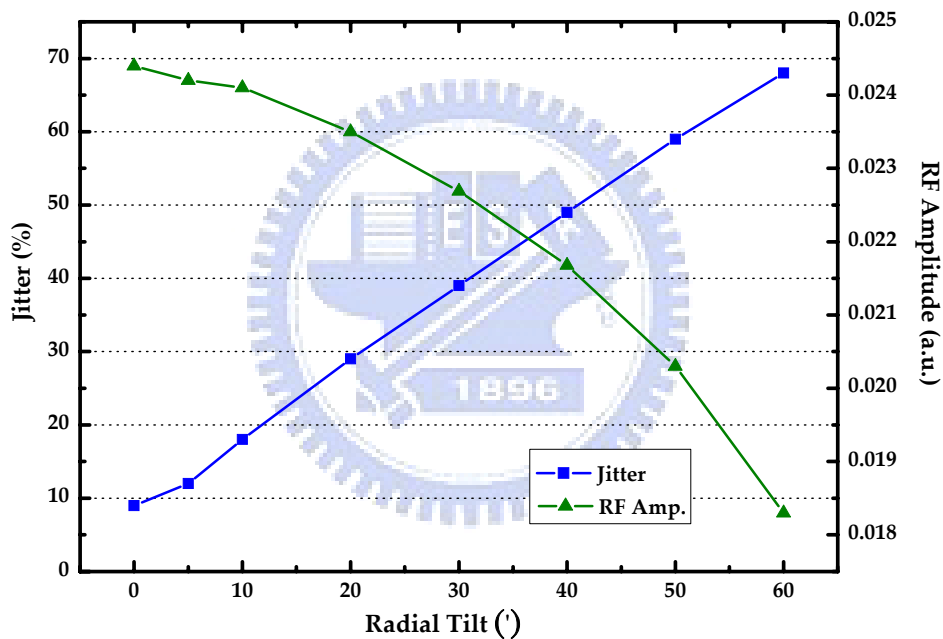


Fig. 4.3-3 The relationship between the radial tilt and the jitter value and the RF amplitude

From Fig. 4.3-3, the decreasing tendency in the amplitude of the RF signal is the same as the results mentioned in Fig. 4.3-2. The reducing amplitude let the photo-detector difficultly to read the returned signal. Meanwhile, the jitter goes up as the function of the tilt angle. The rising jitter result in the misjudgment of length of the original signal, e.g. the mark length of 3T maybe

regard as 4T. This leads to the readout error during reading the disc.

There are two directions of tilt in the ODS system: the radial tilt and the tangential tilt. The plot in Fig. 4.3-4 shows the experimental results of the amount of jitter versus the corresponding tilt directions. As depicted in Fig. 4.3-4, the radial tilt has lower jitter value than the tangential tilt at the same tilt angle. This implies that the optical drive can endure larger tilt angle in the radial direction than in the tangential direction. The reason why the radial direction has a larger tolerance lies in the aberration caused by the tilt. The aberration formed by the tangential tilt leads to a tail of the laser spot in the direction along the track which is reading. The tailed laser spot will illuminate the mark nearby and make the reflected intensity distribution altered. The change impact on the shape of the readout signal of each mark length and generate a larger jitter value.

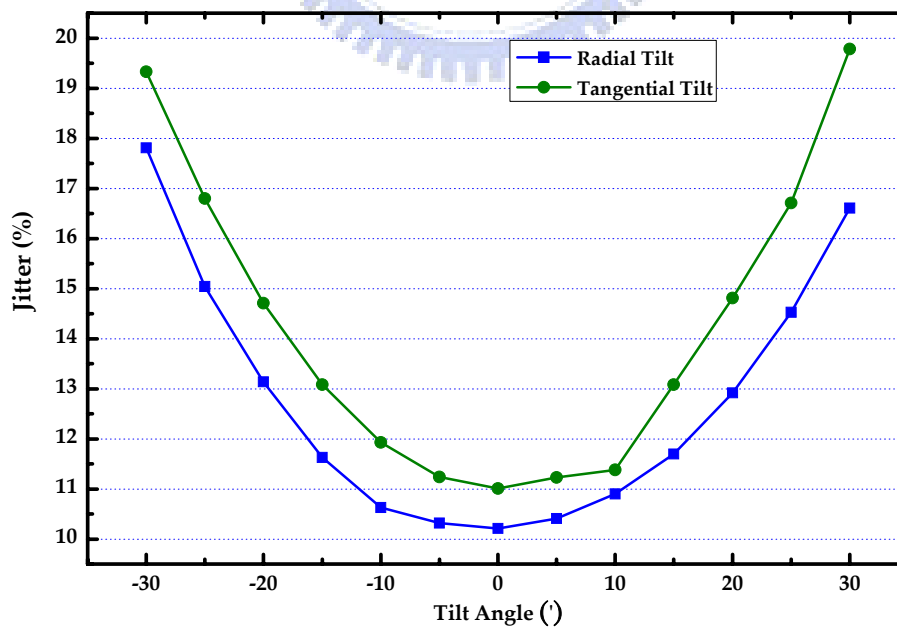


Fig. 4.3-4 The influence of the radial and tangential tilt on the jitter (DVD+R)

4.3.2 Defocus

In our simulation, the process is divided into two steps. At the first stage, the disc is moved in the axial direction to generate a FES. The definition of defocus used in this simulation is modified from that of the original optical drives. To simplify the problem this study assumes that the position of the minimum jitter is coincident with the zero crossing point of the FES without losing the accuracy. This assumption is under the condition that all the other imperfections are eliminated except the defocus.

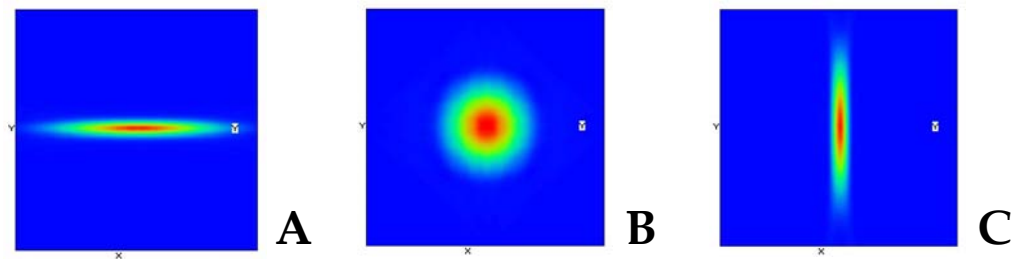
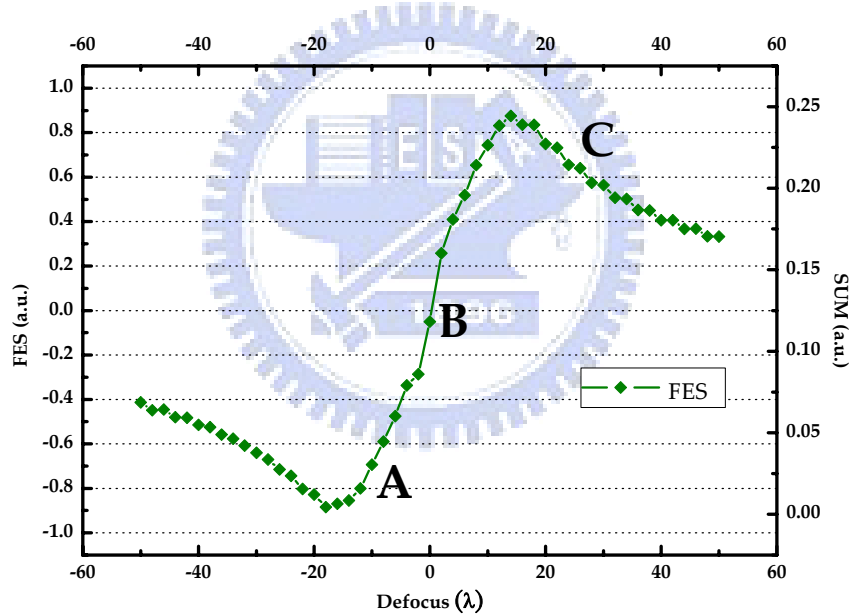


Fig. 4.3-5 The linear range of the FES and the three cross-sections of the intensity distributions at A. too-near, B. in-focus, and C. too-far positions

The linear range of the FES from point A to point C is indicated in the Fig. 4.3-5. The minimum (point A) and maximum (point C) of the FES are at 4603λ and 4635λ , and the in focus position is 4621λ . Note that the linear range is not symmetric at the zero point B.

At the second stage, the disc is moved within the linear range from point A to C to simulate the movement of the objective lens. The jitter of marks of $3T$ is measured and the jitter value is graphed as a function of the defocus in the two opposite directions, as shown in Fig. 4.3-6. It is known that the lowest jitter is located at the focal point as shown in the simulation result. The defocus also leads to an increasing jitter with the distance from the focal point.

The experimental result of the jitter versus the defocus is shown in Fig. 4.3-7. Note that the defocus is defined as the percentage of the offset which is defined in (3.3-4) and the jitter is measured by the TIA method. Although the definition is different, that compared Fig. 4.3-6 with Fig. 4.3-7 demonstrates a close agreement in the shape of the plot. The tendency of the jitter affected by the defocus effect can be simulated with the proposed model.

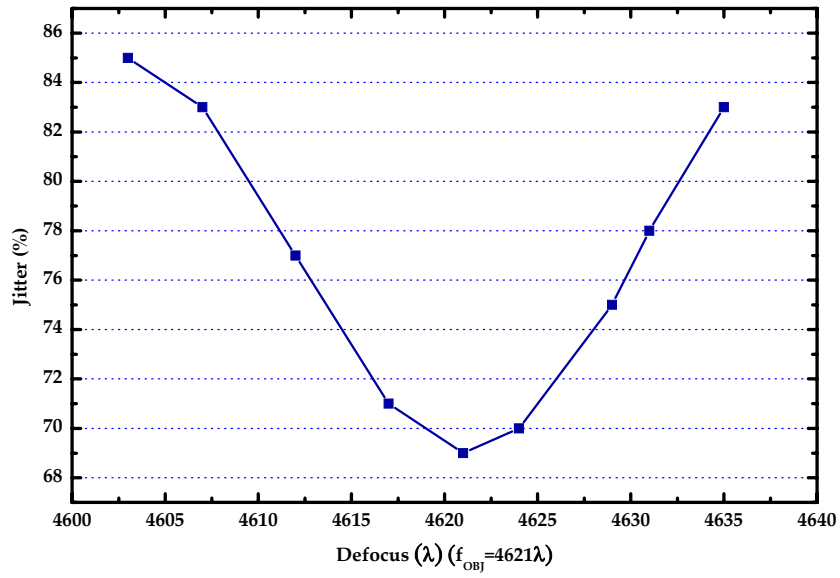


Fig. 4.3-6 The simulated jitter value as a function of the defocus distance

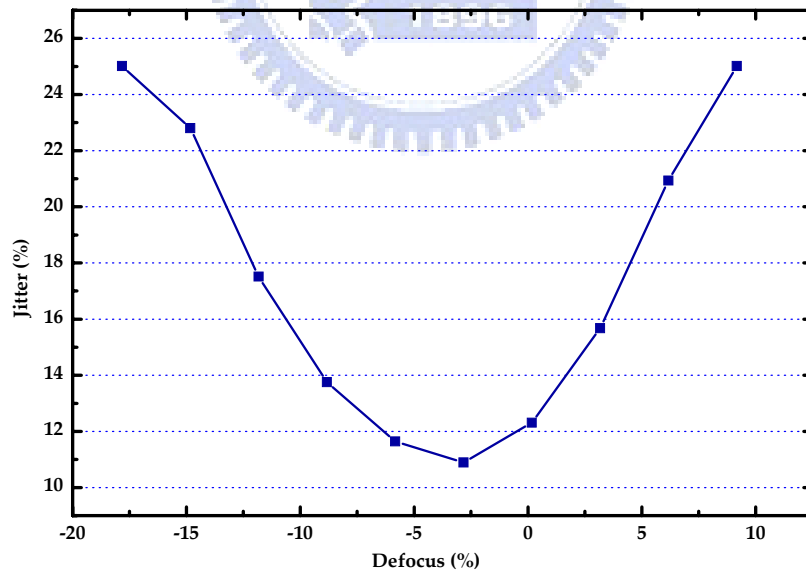


Fig. 4.3-7 The experimental jitter value as a function of the defocus distance

4.4 Results 4 – The Crosstalk between FES & TES: Feedthrough

Two servo mechanisms in the ODS drive, the focus servo and the tracking servo, are usually embodied with the common optical path, and share the same detector. In an ideal drive, these two signals should be mutually independently, e.g. a disturbance of track seeking should not affect the FES and vice versa. But the crosstalk between the FES and the TES is always present, even in an ideal system. In the final part of this thesis, the dependency of the feedthrough on the intensity distribution of the light beam on the photo-detector and the origins of the feedthrough are studied.

The feedthrough will impact the reliability of all kinds of focus-servo and tracking-servo systems in use today. However, this thesis will focus on the astigmatism focus servo method which is the most commonly used in the ODS system, as shown in Fig. 4.4-1.^{[17][18][19]}

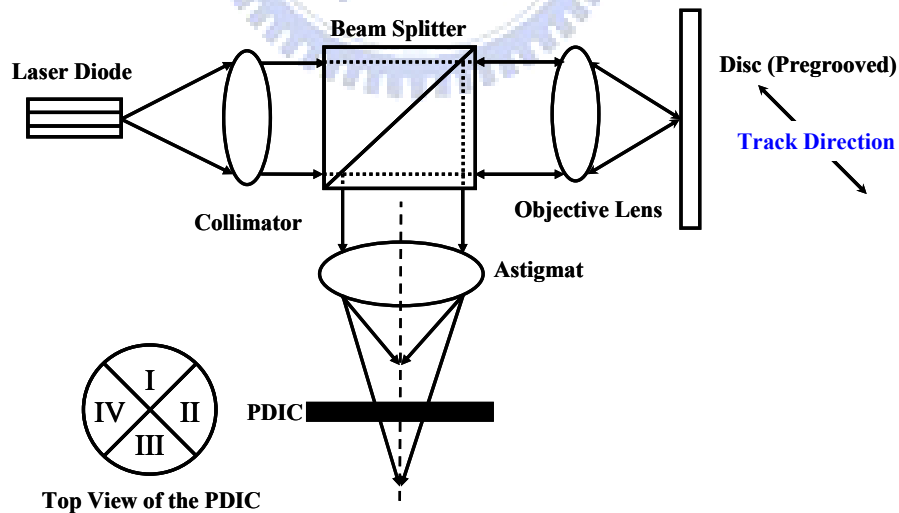


Fig. 4.4-1 The astigmatism focus servo method and the layout of the track direction and photo-detector

The light is focused by the objective lens onto the grooved disc. The reflected light is collimated again and brought to the astigmatic lens whose axis is at 45° to the x-axis to generate two foci and to focus the light onto the photo-detector located at the midpoint of the two foci. When the spacing between the disc and the objective lens is moving away from the optimum value, the intensity distribution on the photo-detector varies with the defocus from circular shape to two perpendicular elliptical shapes.

The key factor of inducing the feedthrough is the grooved optical disc, which acts like a diffraction grating. The diffraction from the edge of the groove and the land leads to different diffraction orders which are the undesired variations for the focus servo system and the cause of the feedthrough. When the light is crossing the tracks, the reflected light diffracts to several order beams which form an interference pattern collected by the objective lens. The amount of the overlapped region depends on the numerical aperture and the diffraction angle of the higher diffraction orders, as shown in Fig. 4.4-2.

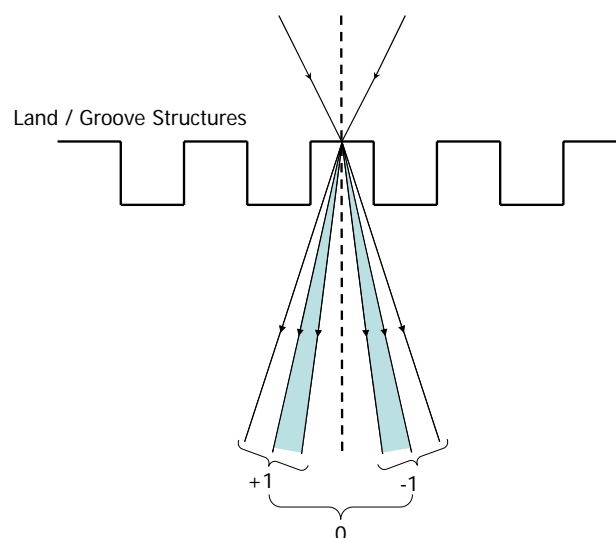


Fig. 4.4-2 The diffraction of the incident wave by the groove structure

The intensity distributions of the overlapped regions are determined by the relative phase difference of the zero order and the ± 1 orders. The intensity distribution on the photo-detector changes as the radial position of the laser spot on the disc moves with respect to the edge of the groove and the land structure. As a result of the track seeking operation, the intensity pattern on the photo-detector varies greatly during the track crossing. This variation infers that even in the ideal (aberration-free) astigmatism focus servo system the feedthrough is always present because of the groove structure of the writable or re-writable discs.

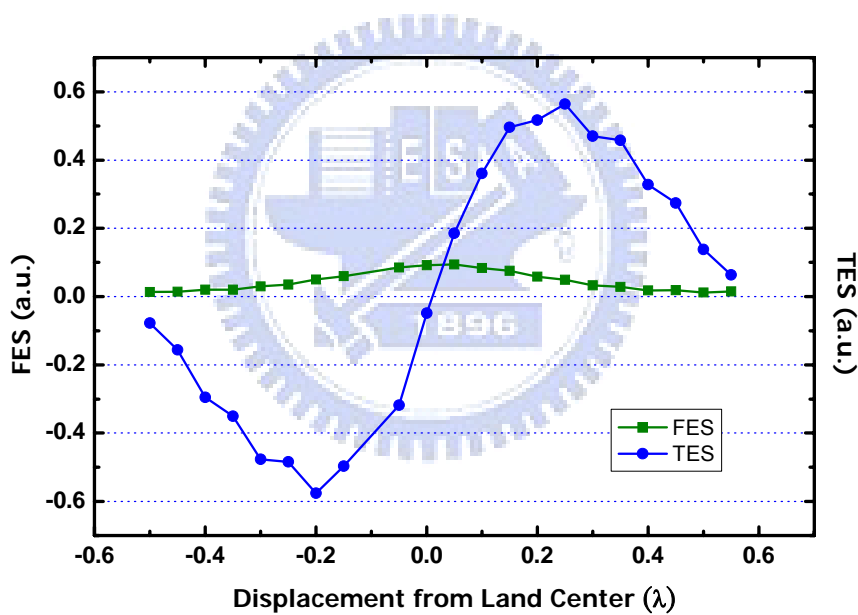


Fig. 4.4-3 The FES and TES of the ideal ODS system with an aberration-free objective lens

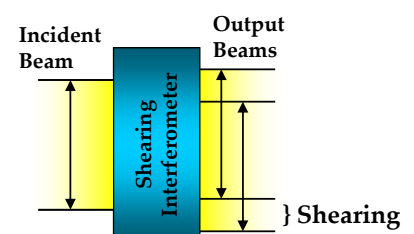
The simulation results of the FES and the TES in an ideal astigmatism focus servo system during track crossing of one trackpitch are shown in Fig. 4.4-3. Compared with the TES, the feedthrough, a false FES, is moderate and tolerable in Fig. 4.4-3 when the laser spot is crossing one trackpitch. Note that

even though the system is ideal, the small amount of feedthrough, the variation of the FES during track crossing, still exists.

The aberrations presented in the ODS system have a large influence on the feedthrough and the degree of influence on the feedthrough depends upon different kinds of aberrations. Because the groove structure on the disc is acted like a shearing interferometer* which produce two laterally shifted diffraction orders that interfere with the zero order beam. The interference pattern in the overlapped region will be easily affected by the aberrations introduced during the propagation. From the prior studies, it is believed that the most common aberrations which will lead to a feedthrough effect are the astigmatic and coma aberrations. Consequently, the effect of these two aberrations on the feedthrough will be simulated and discussed.

The first introduced aberration is coma aberration which is oriented with its tail perpendicular to the track and such aberration can be induced by the disc tilt or the surface variation of the substrate. Fig. 4.4-4 shows the simulation results of the TES and the feethrough (a false FES) with 0.25λ coma aberration. The shape of the TES is distorted by adding the coma aberration on the objective lens. The tail lies in the radial direction which make the zero point of the TES no longer located at the groove or land center. Nevertheless, the effect of coma upon the feedthrough is insignificant.

* Shearing interferometers produce two beams which are laterally shifted. Interference fringes can only be observed in the overlapped region. The fringes in the interferogram indicate curves of constant optical path difference between the doubled and shifted wavefronts.



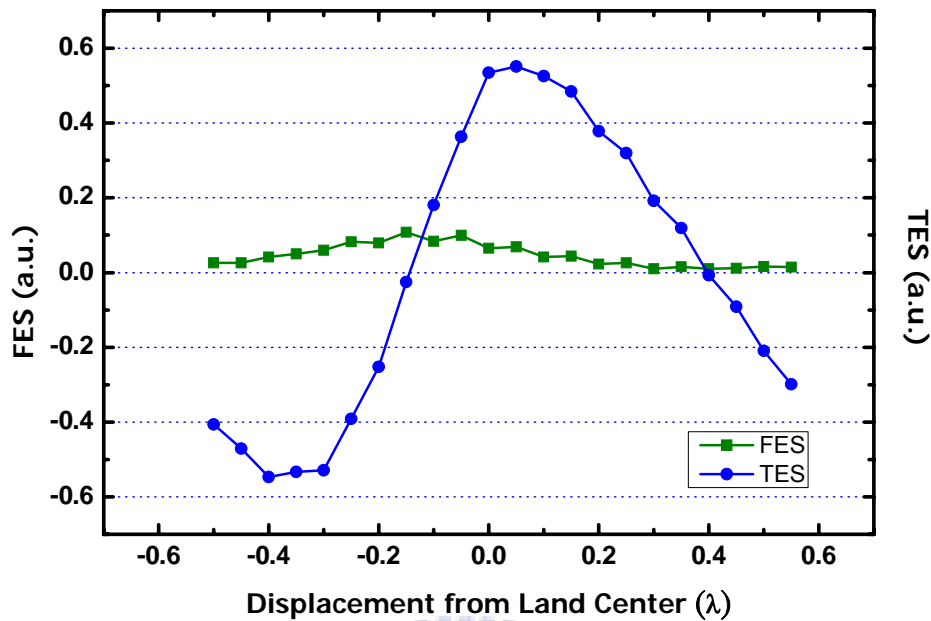


Fig. 4.4-4 The FES and TES of the ODS system with an objective lens of 0.25λ coma aberration

As mentioned in the previous literature, the most serious situation which deteriorate the feedthrough is when the astigmatic line foci are oriented $\pm 45^\circ$ with the track.^[18] The astigmatism which is parallel or perpendicular to the track has a minor influence on the feedthrough. Fig. 4.4-5 demonstrates the worst case of the feedthrough induced by the 45° astigmatism. The peak-to-peak value of the feedthrough is in the same order to the TES. This causes the focus servo to react to this feedthrough level but in fact the laser spot is focused on the desired information layer.

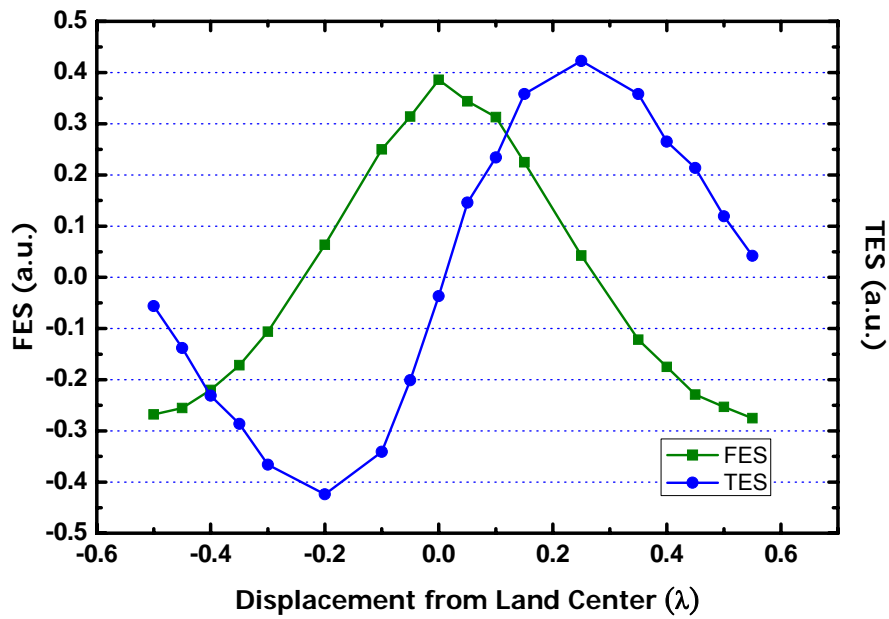


Fig. 4.4-5 The FES and TES of the ODS system with an objective lens of 0.25λ astigmatism aberration

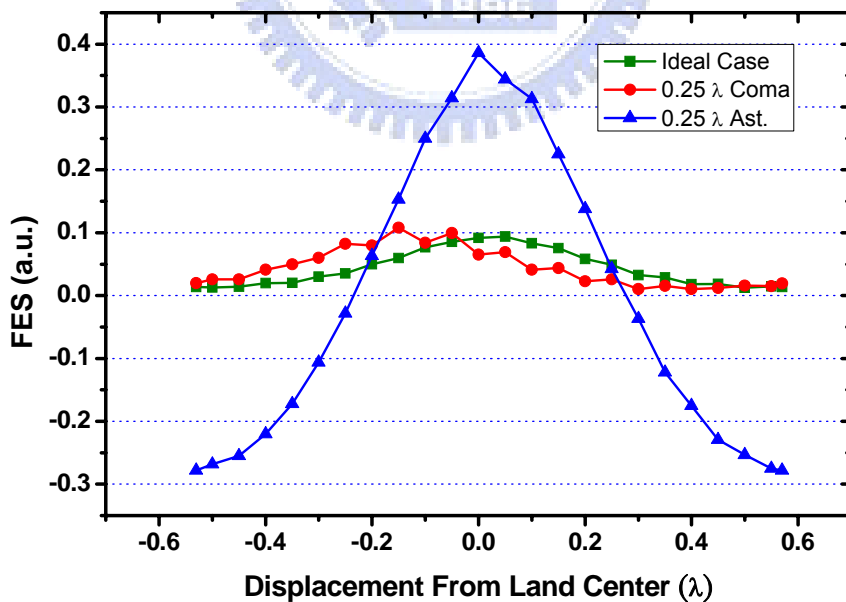


Fig. 4.4-6 The comparison of the false FES (feedthrough) with different conditions

The comparison of the feedthrough with three conditions is graphed in Fig. 4.4-6. This figure confirms the fact that the 45 degrees astigmatism has much larger impact on the feedthrough. The extremes of the feedthrough correspond to the track center and the groove center.

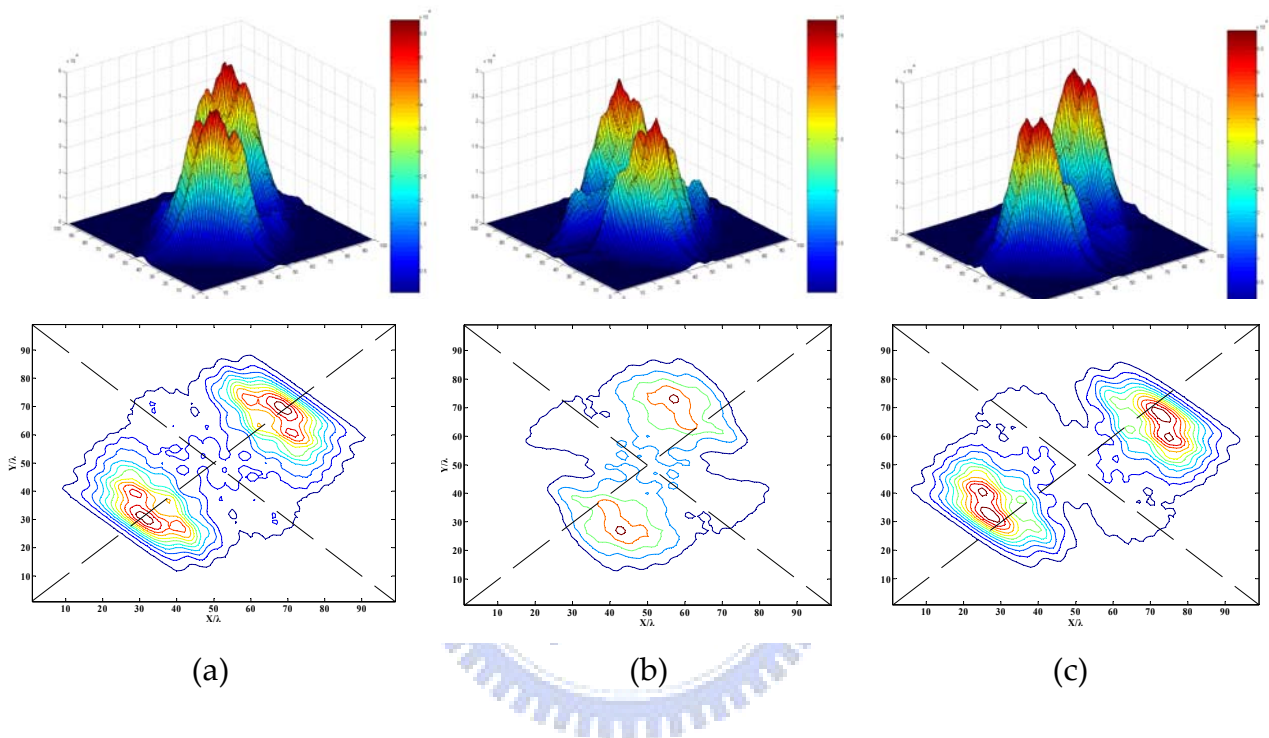


Fig. 4.4-7 The simulated intensity distributions and the contours on the photo-detector for (a) ideal case and two extremes of the feedthrough signal with astigmatism aberration: (b) at the land center, and (c) at the groove center

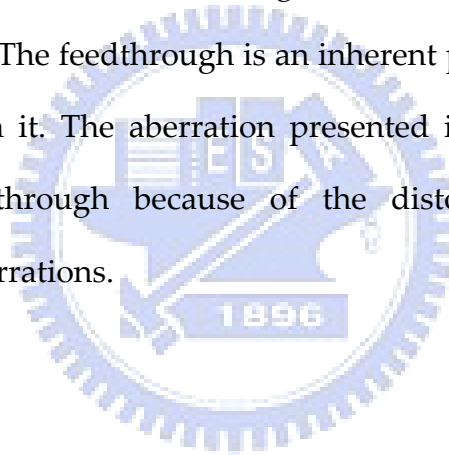
From Fig. 4.4-6, the extreme positions of the feedthrough occur at the groove/land center and the intensity distributions and the contour plots on the photo-detector at these positions are plotted in the Fig. 4.4-7. The results in Fig. 4.4-7(a) are ideal case when the objective lens is free from aberrations for reference. Note that by superimposing the photo-detector boundaries upon the contour plots, one can observe that the intensity distribution is symmetric with the boundaries of the photo-detector. The symmetry of the intensity

pattern on the photo-detector plays an important role on the generation of the feedthrough. The plots of Fig. 4.4-7(b) and (c) where the laser spot are located on the groove and land center show the obviously asymmetric properties with the detector boundaries. The asymmetrical diagonal intensity distribution of the returning beam owing to the groove structure of the disc leads to a more serious false FES. The phase of the returning beam during the seek operation is shown to have a negligible effect on feedthrough for the astigmatic method.



4.5 Summary

The readout signals of the ODS system are obtained by superposing the isolated marks and successfully demonstrated the validity of the proposed readout model. Two servo signals are also acquired by the astigmatism and push-pull method and tested with the specification for correctness. The tilt effect in the ODS system results in the increasing in jitter and the decreasing in amplitude of the eye-pattern, respectively. The plot of the defocus versus the jitter is compared between the simulation and experiment results and shows a close agreement. The feedthrough are introduced and discussed at the end of **Chapter 4**. The feedthrough is an inherent problem of the disc with grooves structures on it. The aberration presented in the ODS system will deteriorate the feedthrough because of the distorted intensity pattern introduced by the aberrations.



Chapter 5

Conclusion and Future Works

5.1 Conclusion

An optical model combined the prior principles in the literatures and innovative approaches to generate the signals in the ODS system was proposed. The proposed model was demonstrated that the simulations and the experiments are in good agreement.

The RF signal is formed by superposition of a sequence of isolated marks of different pit lengths with varied land spacing offsets and overlapping the signals of the isolated marks more than 300 times to obtain the a close result compared with the experiment. The simulated RF signal has a better amplitude ratio (73.58%) than the experimental result (39.20%). Because the simulation model is ideal, which are no aberrations or tolerance issue are considered, the simulation results shown the higher signal contrast ratio make sense. The RF signal from the experiment has a better beta value (8.50%) than the simulation result (13.21%). The overlapping sequence can not simulate the situation of the real case in an accurate way, and therefore the balance between the pits and lands of the simulation result is poorly compared with the real case. The FES and TES are checked with the specification requirements for validity. The linear range of the experiment and the simulation results show the linear range of the simulation model (14.5λ) can satisfy the condition of the experiment (15λ).

The tolerance issues are combined into analysis. The tilt effects introduced by the objective or disc are incorporated into the objective lens. The tilt gives rise to the increasing in the jitter value and the decrease in amplitude of the readout signals. The jitter increases 3.55x and the amplitude of the eyepattern decreases 0.45x. The rising jitter results in the misjudgment of length of the original signal and cause the readout error during reading the disc. The radial tilt has lower jitter value than the tangential tilt at the same tilt angle. This implies that the optical drive can endure larger tilt angle in the radial direction than in the tangential direction. The defocus should be measured and adjusted before the readout process to attain maximum readout amplitude. Although the definition used in the proposed model is different from the traditional optical drive, the results show the good tendency of the jitter with respect to the defocus.

The feedthrough is an inherent problem of the recordable disc with groove structures. The aberrations presented in the ODS system will deteriorate the feedthrough because of the distorted intensity pattern introduced by the aberrations. The most serious situation happens when the astigmatism of the spot inclines 45° to the track. By superimposing the quadrant photo-detector boundaries on the contour plots, the cause of large feedthrough is easier to visualize. Because the FES is the difference of the diagonal sum, the asymmetry in the diagonal direction will lead to a serious feedthrough effect. The phase of the returning beam during the seek operation is shown to have a negligible effect on feedthrough for the astigmatic method.

5.2 Future Works

The kernel of the future work lies in the transition of optical model from DVD system to the higher capacity system, such as Blu-ray and HD-DVD systems. As illustrated in Fig. 5.2-1, the trackpitch the minimum mark length and the thickness of the cover layer are narrowed down to 0.32, 0.15 and 0.1mm, respectively. Reducing the trackpitch and pit length, Blu-ray disc (25GB) realizes around 5 times as much recording capacity as DVD (4.7GB). The lengths adopted in the model are normalized by the wavelength of the laser diode by the software, and therefore the transition of the dimension would be easy for upgrade. But the system in the Blu-ray or HD-DVD are much more complicated compared with the DVD system, the optical model should be constructed with more effort.

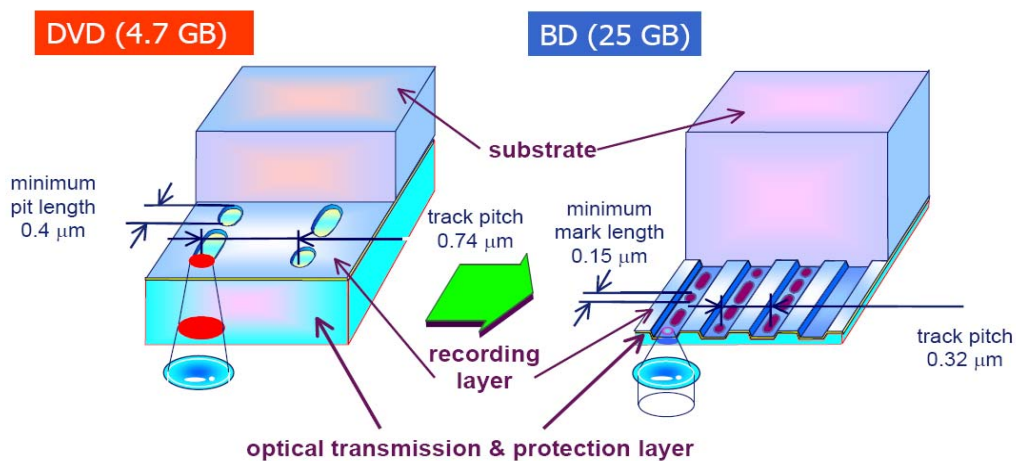


Fig. 5.2-1 Blu-ray disc technology ^[20]

The tolerance becomes an issue when the dimension of the disc is changed. The tilt effect of the Blu-ray system can be maintained to the same order for disc tilt as DVD by adopting a 0.1mm optical transmittance protection layer.

The tolerance of the disc flatness increases 1.3x and the relative cover thickness decreases 0.9x compared with the DVD system due to the smaller cover layer of the Blu-ray disc.^[20]

The servo mechanisms used in the advanced ODS system are different and the various detection schemes, such as differential phase detection (DPD) method, and differential push-pull method can be extended for the future studies.



Reference

- [1] Joseph Braat, Peter Dirksen, Augustus J.E.M. Jansen, "Diffractive read-out of optical discs."
- [2] H. H. Hopkins, "Diffraction theory of laser read-out systems for optical video discs", J. Opt. Soc. Am., Vol.69, No. 1, P.4-24 (1978)
- [3] M. Mansuripur, "The physical principles of magneto optical data recording," Cambridge, Cambridge University Press (1995)
- [4] M. Mansuripur, "Classical Optics and its applications," Cambridge, Cambridge University Press (2002)
- [5] Yoshinori Honguh, "Readout Singal Analysis of Optical Disk Based on Approximated Vector Diffraction Theory," Jpn. J. Appl. Phys., Vol. 42, P.735-739
- [6] T.Milster, "New way to describe diffraction from optical disks", Appl. Opt., Vol. 37, No. 29, P.6878-6883 (1998)
- [7] Joseph W. Goodman, "Introduction to Fourier Optics," New York, McGraw-Hill (1996)
- [8] M. Born, E. Wolf, "Principles of Optics," Cambridge University Press (1999)
- [9] F. L. Pedrotti, L. S. Pedrotti, "Introduction to Optics," Prentice-Hall, P.388 (1993)
- [10] P. Asthana, B. I. Finkelstein, A. A. Fennema, "Rewritable Optical disk drive technology," IBM J. RES. DEVELOP., Vol. 40, No. 5, P.543-558 (1996)
- [11] J. Braat, "Influence of Substrate thickness on Optical Disk Readout," Appl. Opt., Vol. 36, No. 30, P.8056-8062 (1997)
- [12] R. E. Gerber, M. Mansuripur, "Tilt Correction in An Optical Disk System," Appl. Opt., Vol. 35, No. 35, P.7000-7007 (1996)
- [13] C. L. Bartlett, D. Kay, M. Mansuripur, "Computer Simulation of Effects of Disk Tilt and Lens Tilt on Push-pull Tracking Error Signal in an Optical Disk Drive," Appl. Opt., Vol. 36, No. 32, P.8467-8473 (1997)
- [14] J. M. Geary, "Introduction to Lens Design," Willmann-Bell, P.65-83 (2002)
- [15] P. W. Nutter, C. D. Wright, "A New Technique for the Prediction and Correction of Nonlinearities in Simulated Optical Readout Waveforms," Proceedings of SPIE, Vol. 4342, P.364-374 (2002)
- [16] DVD+Recordable Basic Format Specifications Ver. 1.2 (2003)
- [17] M. R. Latta, T. C. Strand, J. M. Zavislan, "Effect of Track rossing on Focus Servo Signal: Feedthrough," SPIE, Vol. 1663, P.157-163 (1992)

- [18] Bruce E. Bernacki and M. Mansuripur, "Causes of focus-error feedthrough in optical-disk systems: astigmatic and obscuration methods," Appl. Opt., Vol.33, No. 5, P.735-743 (1994)
- [19] B. E. Bernacki, K. Bates, M. Mansuripur, D. Hansen, D. Cisneros ,
"Characterization of a novel focusing/tracking technique with increased feedthrough immunity for optical-disk applications: the double-astigmatic method," Appl. Opt., P.5789-5796 (1993)
- [20] J. Heemskerk, "Blu-ray Disc: A Disruption or a Next Step in Evolution?,"
PHILIPS

